Modeling shear bands in J_2 plasticity using a two-scale formulation via embedded strong discontinuity modes

Sebastián D'hers[(1)] and Eduardo N. Dvorkin[(2)*]
[(1)]Instituto Tecnológico de Buenos Aires
Av. E. Madero 399
C1106ACD, Buenos Aires, Argentina
[(2)]IMATEC, Engineering School, University of Buenos Aires
Av. Las Heras 2214, C1127AAR Buenos Aires, Argentina
SIM&TEC
Av. Pueyrredón 2130, C1119ACR Buenos Aires, Argentina

Abstract

A new two-scale finite element formulation was developed for modeling J_2 plastic deformation processes ($2D$) in which shear band localizations take place. The formulation is based on the use of embedded strong discontinuity modes which are triggered using a stress based criterion. The new formulation does not require a specific mesh refinement to model the localization phenomena and provides mesh independent results. The shear bands constitutive behavior is derived from the continuum properties without the introduction of any ad hoc physical law.

Keywords: plasticity, localization, shear band, strong discontinuity, multiple scales formulation

1 Introduction

During the plastic deformation of metals, under certain stress/strain conditions, a very narrow localized zone of intense plastic shearing can occur: this phenomenon is called shear banding and has been profusely described in the mechanics literature [1]-[4].

A theoretical elastoplastic analysis using the J_2 plasticity model indicates that the shear bands are localized along a line (zero width) and that the phenomenon is associated with a loss of uniqueness in the problem solution.

The difficulty in modeling shear banding processes using J_2 plasticity and standard finite element formulations lies in the different scales that need to be used for the description of the global deformation in the continuum and the localized deformation along zero width lines.

When standard finite element formulations are used for modeling plastic deformation processes in which shear bands are present, the width of the shear bands is forced to be in the elements size scale.

*Corresponding author. Email: edvorkin@fi.uba.ar

To illustrate on the results that are obtained when using standard finite element formulations for modeling shear banding processes, in what follows we discuss two examples: in Fig. 1 we present the results obtained modeling an elastoplastic plane strain sample under tension in which a shear band develops: while the Q1-P0 element [5] cannot predict the shear band localization, diffusing therefore the deformation over a width comprising several elements, the QMITC element [6] [7] localizes the shear band in one element; however, even in this optimum case the solution is mesh dependent because the element size controls the shear band transversal dimension; in Fig. 2 we present the QMITC results for the modeling of a threaded coupled connection in a steel pipe; the shear band is localized in one element. We also show in Fig. 3 an etched sample showing the actual localized deformation.

1.1 Background

For introducing the localization phenomenon in the finite element models several strategies have been developed; in Fig. 4 we present a schematic representation of them:

- Using a continuous displacement field: as it was discussed above the results are mesh dependent; the elements formulation plays an important role in defining the capability for localizing the plastic deformations [8].
- Introducing a weak discontinuity in the elements displacement field ($d > 0$ but small) [9].
- Introducing a strong discontinuity in the elements displacement field [10] [11].

Two kind of localization problems should be distinguished: fracture in brittle materials and shear-band deformation in ductile metals. For both cases, once the localization is triggered almost all the deformation concentrates in a narrow band. The triggering of the localization and the post-localization behavior are described, in both cases, by different models.

1.1.1 Brittle fracture

For modeling the fracture of brittle materials like concrete, rocks and ceramics, the fracture initiation is defined by a tensile stress larger than a threshold value and during fracture propagation we can observe a softening in the load-displacement response; since a local constitutive relation showing strain softening was proved to be thermodynamically unacceptable [12] [13] the phenomenon is modeled introducing a fractomechanics concept: the fracture energy, which has been shown to be a material property [14] - [19]. The different finite element methodologies that were developed for modeling the fracture process in brittle materials are [20]: the smeared crack approach [17], [21]-[24]; the discrete crack approach [25] [26]; finite elements with embedded discontinuous strain fields [9] [27], finite elements with embedded discontinuous displacement fields [10] [11] [28] [29] and the micropolar continuum theory [30] [31].

1.1.2 Shear bands

Regarding the shear-banding of elastoplastic materials, localization implies that the acoustic tensor becomes singular [32]-[34]. For this to happen the material is required not to harden, [33]. For materials following the von Mises (J_2) associated plasticity model, the shear bands initiation and propagation are discussed in the second section of this paper. Many techniques have been proposed for shear band modeling:

- Enhanced strain field. First introduced in [9] the strain field was enhanced with a jump function within each element crossed by the localization line. Many other enhancements were proposed, see [20], [35]-[37].
- Extended finite element method (X-FEM). In Ref. [38] the authors enriched the finite element interpolations near a crack by incorporating a discontinuous field through a partition of unity method; this procedure was applied recently for the spatial discretization of the governing equations of shear bands treated as strong discontinuities together with an embedded traction separation law applied to cohesive surfaces [39]. In [40], focused on dynamic problems, the plastic evolution of the material that surrounds the shear band is modeled enhancing the finite element interpolation with a fine scale strain function.
- Unfitted finite elements techniques introduced in [41] [42] , have been used for shear bands in Refs. [43] [44], where additional degrees of freedom are added to the nodes belonging to the elements crossed by the discontinuity.

1.2 Our new formulation

Our objective in the present paper is to introduce a new two-scale finite element formulation to model, using J_2 plasticity, deformation processes that develop shear banding.

The constraints that we impose on our new formulation are:

1. It should not require a specific mesh refinement to model the localization phenomena and it should provide mesh independent results.
2. Perfect plastic materials should not require the use of softening laws to localize, because softening material properties have not been defined nor measured in the environment of J_2 plasticity.

In the second section of this paper we review the conditions for the triggering of the shear banding process and we formulate a stress based criterion. In the third section we present our new finite element formulation for modeling shear band deformations. This new formulation incorporates a second scale via ad hoc consideration of the displacement localization modes and it is based on the formulation of the embedded localization lines [10] [11].

In the fourth section we present the numerical results that we obtained using our new formulation and we show that it can model shear band localizations without introducing a softening stress/strain relation providing mesh independent results. We also show that the results that we produce using our new formulation are convergent when the mesh is refined even if a softening stress/strain relation is used.

2 Shear bands inception: a stress based criterion

During the elastoplastic deformation of a solid, considering the J_2 associated plasticity model, the following equations apply [45],

$$
\begin{aligned}
{}^t\sigma_{ij} &= {}^tC^E_{ijkl}\,({}^t\varepsilon_{kl} - {}^t\varepsilon^P_{kl}) && \text{(1a)}\\
{}^t\varepsilon^P_{kl} &= {}^t\lambda\frac{\partial\,{}^t f}{\partial\sigma_{kl}} && \text{(1b)}\\
{}^t f &= \frac{3}{2}\,{}^t s_{ij}\,{}^t s_{ij} - {}^t\sigma_y^2 = 0\,. && \text{(1c)}
\end{aligned}
$$

In the above equations, written in a Cartesian coordinate system for infinitesimal strains and isotropic hardening, ${}^t\sigma_{ij}$ are the components of the Cauchy stress tensor at time (configuration) t, ${}^tC^E_{ijkl}$ are the components of the fourth order elastic constitutive tensor, ${}^t\varepsilon_{kl}$ are the components of the deformation tensor, ${}^t\varepsilon^P_{kl}$ are the components of the plastic deformation tensor, ${}^ts_{ij}$ are the components of the deviatoric part of the Cauchy stress tensor, ${}^tf = 0$ is the yield function and ${}^t\sigma_y$ is the yield stress.

In a $2D$ geometry, a shear band can be characterized by a line with normal ${}^t\underline{\mathbf{n}}$**,** the direction of the displacement jump $[[{}^t\underline{\mathbf{u}}]]$**,** which we call ${}^t\underline{\mathbf{m}}$ and a scalar bandwidth d as proposed in [33] [34]. In Fig. 5 we draw a schematic representation of the above definitions, considering that the displacement jump in the shear band is in the tangential direction (mode II) and $d = 0$.

It has been shown [32] that the band orientation can be determined from the singularity of the acoustic stress tensor, since the vanishing of the determinant of the acoustic tensor at any point in the elastoplastic continua indicates the fulfillment of the necessary bifurcation condition.

The elastoplastic constitutive tensor [46] is, for perfect plasticity

$$
{}^t\underline{\underline{\underline{\underline{\mathbf{C}}}}}^{\mathbf{EP}} = \left(\kappa - \frac{2}{3}G\right)\,{}^t\underline{\underline{\mathbf{g}}}\;{}^t\underline{\underline{\mathbf{g}}} + 2G\,{}^t\underline{\underline{\underline{\underline{\mathbf{I}}}}}^4 - 2G\,\frac{{}^t\underline{\underline{\mathbf{s}}}\,{}^t\underline{\underline{\mathbf{s}}}}{{}^t\underline{\underline{\mathbf{s}}} : {}^t\underline{\underline{\mathbf{s}}}} \tag{2}
$$

where ${}^t\underline{\underline{\mathbf{s}}}$ is the deviatoric stress tensor, κ the elastic bulk modulus, G the elastic tangential modulus, and

$$
{}^t\underline{\underline{\underline{\underline{\mathbf{I}}}}}^4 = \frac{1}{2}\left({}^tg^{ik}\,{}^tg^{jl} + {}^tg^{il}\,{}^tg^{jk}\right)\,{}^t\underline{\mathbf{g}}_i\,{}^t\underline{\mathbf{g}}_j\,{}^t\underline{\mathbf{g}}_k\,{}^t\underline{\mathbf{g}}_l \tag{3}
$$

is the symmetric fourth order identity tensor. In these equations we indicate the tensorial product between two tensors as $\underline{\underline{ab}}$ (in other references it is indicated as $\underline{\underline{a}}\otimes\underline{\underline{b}}$).

In [32] it is defined the acoustic constitutive tensor in a direction ${}^t\underline{\mathbf{n}}$ as,

$$
{}^t\underline{\underline{\mathbf{Q}}} = {}^t\underline{\mathbf{n}}\cdot{}^t\underline{\underline{\underline{\underline{\mathbf{C}}}}}^{\mathbf{EP}}\cdot{}^t\underline{\mathbf{n}} = \left(\kappa - \frac{2}{3}G\right)\,{}^t\underline{\mathbf{n}}\cdot\,{}^t\underline{\underline{\mathbf{g}}}\;{}^t\underline{\underline{\mathbf{g}}}\cdot\,{}^t\underline{\mathbf{n}} + 2G\;{}^t\underline{\mathbf{n}}\cdot\,{}^t\underline{\underline{\underline{\underline{\mathbf{I}}}}}^4\cdot\,{}^t\underline{\mathbf{n}} - \frac{2G}{{}^t\underline{\underline{\mathbf{s}}} :\, {}^t\underline{\underline{\mathbf{s}}}}\,{}^t\underline{\mathbf{n}}\cdot\,{}^t\underline{\underline{\mathbf{s}}}\,{}^t\underline{\underline{\mathbf{s}}}\cdot\,{}^t\underline{\mathbf{n}}. \tag{4}
$$

After some algebra we get,

$$
{}^t\underline{\underline{\mathbf{Q}}} = \left(\left(\kappa - \frac{2}{3}G\right)\,{}^tn_j\,{}^tn_k + G\;{}^tn_i\;(\delta_{ik}\delta_{jl} + \delta_{il}\delta_{jk})\;{}^tn_l - \frac{\mathbf{2}G}{{}^t\underline{\underline{\mathbf{s}}} :\, {}^t\underline{\underline{\mathbf{s}}}}\,{}^tn_i\,{}^ts_{ij}\,{}^ts_{kl}\,{}^tn_l\right)\,{}^t\underline{\mathbf{e}}_j\;\;{}^t\underline{\mathbf{e}}_k \tag{5}
$$

where ${}^t\underline{\mathbf{e}}_j$ are the unit base vectors of a Cartesian system.

To investigate the stress state that produces the necessary localization condition we define a new Cartesian coordinate system $\widehat{x}_i$ with $\widehat{x}_1$ in the ${}^t\underline{\mathbf{n}}-$direction and $\widehat{x}_2$ in the ${}^t\underline{\mathbf{m}}-$direction. In this system we write,

$$\det\left({}^t\hat{Q}_{jk}\right) = \det\left(\left(\kappa - \frac{2}{3}G\right)\ {}^t\hat{n}_j\ {}^t\hat{n}_k + G\ \ {}^t\hat{n}_i\ \left(\delta_{ik}\delta_{jl} + \delta_{il}\delta_{jk}\right)\ {}^t\hat{n}_l - \frac{2G}{{}^t\underline{\underline{\mathbf{s}}} :\ {}^t\underline{\underline{\mathbf{s}}}}\ {}^t\hat{n}_i\ {}^t\hat{s}_{ij}\ {}^t\hat{s}_{kl}\ {}^t\hat{n}_l\right) \tag{6}$$

and,

$$\det\left({}^t\hat{Q}_{jk}\right) = \frac{1}{3}G^2\frac{(3\kappa - 2G)\ {}^t\hat{s}_{11}^2 + (3\kappa + 4G)\ {}^t\hat{s}_{22}^2 + (3\kappa + 4G)\ {}^t\hat{s}_{33}^2 + (6\kappa + 8G)\ {}^t\hat{s}_{23}^2}{{}^t\underline{\underline{\mathbf{s}}} :\ {}^t\underline{\underline{\mathbf{s}}}}. \tag{7}$$

For the fulfillment of the localization condition — $\det\left({}^t\hat{Q}_{jk}\right) = 0$ — we must have ${}^t\hat{s}_{11}^2 = {}^t\hat{s}_{22} = {}^t\hat{s}_{33} = {}^t\hat{s}_{23} = 0$. For a hydrostatic state these equations are fulfilled but when we calculate the value of $\det({}^t\hat{Q}_{jk})$ while reaching a hydrostatic stress state, we get an indetermination that we solve by taking directional limits; for example,

$$\lim_{{}^t\hat{s}_{11} \to\, 0\, {}^t\hat{s}_{22} = {}^t\hat{s}_{33} = {}^t\hat{s}_{12} = {}^t\hat{s}_{13} = {}^t\hat{s}_{23} = 0} \det\left(\widehat{Q}_{jk}\right) = \frac{1}{3}G^2\left(3\kappa - 2G\right)\cdot \tag{8}$$

When we perform the above calculation along all possible directions we find values ranging from $\frac{1}{3}G^2\left(3\kappa - 2G\right)$ to $\frac{1}{3}G^2\left(6\kappa + 8G\right)$ but for all cases $\det\left(\widehat{Q}_{jk}\right) > 0$, so no localization is possible. Hence to have localization we must have either ${}^t\hat{s}_{12}^2 \neq 0$ or ${}^t\hat{s}_{13}^2 \neq 0$ or both. Therefore, for J_2 plasticity,

a) The localization criteria based on stress components is that the stress tensor ${}^t\underline{\underline{\boldsymbol{\sigma}}}$ must be able to fulfill the above conditions for an orientation $\hat{\mathbf{x}}$.

b) The localization condition only depends on the current stress state.

c) The localization direction will lie in a plane orthogonal to one of the stress principal axes, since ${}^t\hat{\sigma}_{23} = 0$.

d) The necessary condition for localization along the directions $(\widehat{x}_{1,2,3})$ is,

$${}^t\widehat{\sigma}_{11} + {}^t\widehat{\sigma}_{22} = 2\,{}^t\sigma_h = 2\,{}^t\widehat{\sigma}_{33} \tag{9}$$

where ${}^t\sigma_h$ is one third of the first invariant of the stress tensor at the point.

e) The sufficient conditions for localization are Eqn. (9) together with,

$${}^t\hat{\sigma}_{12} \neq 0 \tag{10}$$

If localization is not reached at plasticity onset, the stress conditions may be fulfilled later on the deformation path.

We now examine the case of a specimen in simple tension. We first consider a plane strain specimen in pure traction along x_1-direction with no restrains in x_2-direction. For this case is has been shown that the out-of-plane stress tends to $\sigma_{33} = \frac{\sigma_{11}}{2}$ as the plastic deformation grows [47]. Using the above discussed localization criteria, we find that for a direction $\widehat{x}_1$ at an angle $\alpha = \frac{\pi}{4}$ with the x_1- direction we fulfill Eqns. (9, 10). The localization is attained in this case after some plastic deformation is developed and the stress state evolves until it satisfies the localization criteria.

Considering an axisymmetric specimen, we find that the only possible non-zero shear strain is,

$${}^t\sigma_{13} \neq 0\ ^1 \tag{11}$$

[1] Here "1" is the radial direction, "2" is the angular direction and "3" is the axial direction.

hence, the localization direction will lie on a radial plane. This assures that the shear band growth will occur under axisymmetric conditions until some instability (buckling) arises forcing the deformation to go out of plane; hence, the modeling of the band growth does not require the use of a more complex and expensive 3D model.

Finally we consider the case of plane stress specimen in tension where, for perfect plasticity, the localization condition in terms of the stress tensor components in the band aligned coordinate system $\widehat{x}$ is,

$$\det\left({}^{t}\widehat{Q}_{jk}\right) = \frac{4G^3\kappa\ \left(2\ {}^{t}\hat{\sigma}_{22} - \ {}^{t}\hat{\sigma}_{11}\right)^2}{(\kappa+G)\ \left({}^{t}\hat{\sigma}_{11}^2 + \ {}^{t}\hat{\sigma}_{22}^2\right) - (\kappa+2G)\ {}^{t}\hat{\sigma}_{11}\ {}^{t}\hat{\sigma}_{22} + (3\kappa+4G)\ {}^{t}\hat{\sigma}_{12}^2} = 0 \tag{12}$$

hence,

$$\left(2\ {}^{t}\hat{\sigma}_{22} - \ {}^{t}\hat{\sigma}_{11}\right)^2 = 0 \Rightarrow \ {}^{t}\hat{\sigma}_{11} = 2\ {}^{t}\hat{\sigma}_{22}. \tag{13}$$

This condition shows no dependence on the shear stress $\hat{\sigma}_{12}$ and it can be fulfilled from the onset of the plastic deformation. Using the components in the global (x_1, x_2) directions, we can calculate the angle α between this global directions and the band oriented $(\widehat{x}_1, \widehat{x}_2)$ directions:

$$\alpha = \begin{cases} \arctan\left(\frac{2\sqrt{9\sigma_{12}^2-5\sigma_{11}\sigma_{22}+2\sigma_{11}^2+2\sigma_{22}^2}-6\sigma_{12}}{2(2\sigma_{11}-\sigma_{22})}\right) \\ \arctan\left(\frac{-2\sqrt{9\sigma_{12}^2-5\sigma_{11}\sigma_{22}+2\sigma_{11}^2+2\sigma_{22}^2}-6\sigma_{12}}{2(2\sigma_{11}-\sigma_{22})}\right) \end{cases} \text{ if } 2\sigma_{11}-\sigma_{22} \neq 0. \tag{14}$$

$\alpha = 0$ otherwise

Solving numerically for a case of simple tension (${}^{t}\sigma_{11} \neq 0\ ;\ {}^{t}\sigma_{22} = 0\ ;\ {}^{t}\sigma_{12} = 0$) we get $\alpha = \pm\,(35.26)\,^{\circ}$, which is the usual value.

2.1 Materials with plastic hardening/softening

For materials with hardening/softening behavior, the fourth order constitutive tensor is [46],

$${}^{t}\underline{\underline{\underline{\underline{\mathbf{C}}}}}^{\mathbf{EP}} = \left(\kappa - \frac{2}{3}G\right)\ {}^{t}\underline{\underline{\mathbf{g}}}\ {}^{t}\underline{\underline{\mathbf{g}}} + \ 2G\ {}^{t}\underline{\underline{\underline{\underline{\mathbf{I}}}}}^{4} - \frac{2G}{1+\frac{H+K}{3G}}\ \frac{{}^{t}\underline{\underline{\mathbf{s}}}\ {}^{t}\underline{\underline{\mathbf{s}}}}{{}^{t}\underline{\underline{\mathbf{s}}}\colon {}^{t}\underline{\underline{\mathbf{s}}}} \tag{15}$$

where H is the isotropic hardening modulus and K is the kinematic hardening modulus.

Particularizing for isotropic hardening we get the localization condition,

$$\frac{1}{3}G^2\frac{G\ (9\kappa-16G)\ {}^{t}\hat{s}_{11}^2 + G\ (9\kappa+12G)\left({}^{t}\hat{s}_{22}^2 + \ {}^{t}\hat{s}_{33}^2 + 2\ {}^{t}\hat{s}_{23}^2\right) + H\ (4G+3\kappa)\ \left[{}^{t}\underline{\underline{\mathbf{s}}}\colon {}^{t}\underline{\underline{\mathbf{s}}}\right]}{(3G+H)\ \left[{}^{t}\underline{\underline{\mathbf{s}}}\colon {}^{t}\underline{\underline{\mathbf{s}}}\right]} = 0. \tag{16}$$

Under hardening conditions, $H > 0$, no localization can take place, but in softening we get from the above that the $H-$value that produces localization is obtained from,

$$H = -3G\frac{\left({}^{t}\hat{s}_{11}^2 + \ {}^{t}\hat{s}_{22}^2 + \ {}^{t}\hat{s}_{33}^2 + 2\ {}^{t}\hat{s}_{23}^2\right)}{\left[{}^{t}\underline{\underline{\mathbf{s}}}:\ {}^{t}\underline{\underline{\mathbf{s}}}\right]} + \frac{6G\ {}^{t}\hat{s}_{11}^2}{(3\kappa+4G)\left[{}^{t}\underline{\underline{\mathbf{s}}}:\ {}^{t}\underline{\underline{\mathbf{s}}}\right]}. \tag{17}$$

For $H = 0$ the above leads to Eqns.(9) and (10).

In Ref. [1] the impossibility of producing shear bands in a material with plastic hardening is discussed on physical grounds.

3 The finite element formulation

In this section we present the finite element formulation that we developed, via a two-scale strategy based on the strong discontinuity approach, for modeling the occurrence of shear bands in $2D$ elastoplastic problems when using the associated J_2 plasticity model.

3.1 The localized scale: strong discontinuity modes

The basis of our formulation is that when within an element the localization indicator triggers the inception of a shear band, we have to introduce in the element displacements interpolation field a sliding discontinuity along the predicted shear band direction; however, if we just make an obvious extension of the formulation developed for frictional materials in [10] - [11], but using instead of the displacement discontinuity in the direction normal to the crack ($^t\underline{\mathbf{n}}$), a displacement discontinuity in the direction tangential to the shear band ($^t\underline{\mathbf{m}}$) we come across a kinematic inconsistency: as shown in Fig. 6, an element sliding along an internal line increases its volume and this volume growth would require the continuous part of the deformation to decrease its volume in order to fulfill the plastic J_2 incompressibility constraint. It is worth noting that when modeling a type I failure mode, as shown in [10] - [11], this volume increase is sought because it is a characteristic of materials with opening cracks.

Hence, at the element were the localization indicator triggers the discontinuity, instead of introducing a displacement jump along a line we introduce a displacement mode that while modeling the local scale of the shear bands behavior avoids the above discussed kinematic inconsistency. For this purpose we use,

$$\underline{\mathbf{U}}=\underline{\mathbf{U}}_{cont}+\underline{\mathbf{U}}_{sb} \tag{18}$$

where in the vector $\underline{\mathbf{U}}$ we have the nodal incremental displacements which are decomposed into: $\underline{\mathbf{U}}_{cont}$, the displacements that model the continuous scale and $\underline{\mathbf{U}}_{sb}$, the displacements that model the shear band localization.

We now introduce,

$$\underline{\mathbf{U}}_{sb} = \gamma\, \underline{\mathbf{\Theta}} \tag{19}$$

where $\underline{\mathbf{\Theta}}$ are the nodal displacements corresponding to the localized deformation pattern, and γ is a scalar parameter which is part of the problem unknowns.

To build $\underline{\mathbf{\Theta}}$, we consider that linear quadrilateral elements have 8 eigenmodes which, in the case of undistorted elements, can be easily decomposed into: 3 rigid body modes, 1 volume change mode, 2 pure bending modes and 2 pure shear modes. Using the two shear modes we can build a base of pure shear modes in the isoparametric natural element space (r, s). Using this *"shear base"* for an undistorted element, we can compose a pure shear eigenmode in any desired direction. However, in the case of a distorted element, the resultant shear mode is associated with a volume change; hence, to enforce the plastic incompressibility, the *"shear base"* is enhanced using the volume change eigenmode . Finally the vector $\underline{\mathbf{\Theta}}$ is determined so as to produce the maximum shear at a direction coincident with the band direction and zero volume change.

To determine $\underline{\mathbf{\Theta}}$ we first work with the 2×2 undistorted 4-node element in the natural coordinates system (r, s), for which in Table I we define the deformed element nodal coordinates, corresponding to the three deformation eigenmodes in the *"shear base"*: the two pure shear modes and the volume change mode, depicted in Fig. 7.

	${}^t\Phi_r^1$	${}^t\Phi_s^1$	${}^t\Phi_r^2$	${}^t\Phi_s^2$	${}^t\Phi_r^3$	${}^t\Phi_s^3$	${}^t\Phi_r^4$	${}^t\Phi_s^4$
${}^t\underline{\mathbf{\Phi}}_I$	$\frac{1}{2}$	$\frac{3}{2}$	$-\frac{1}{2}$	$\frac{3}{2}$	$-\frac{1}{2}$	$-\frac{3}{2}$	$\frac{1}{2}$	$-\frac{3}{2}$
${}^t\underline{\mathbf{\Phi}}_{II}$	$\frac{3}{2}$	$\frac{3}{2}$	$-\frac{1}{2}$	$\frac{1}{2}$	$-\frac{3}{2}$	$-\frac{3}{2}$	$\frac{1}{2}$	$-\frac{1}{2}$
${}^t\underline{\mathbf{\Phi}}_{III}$	$\frac{3}{2}$	$\frac{3}{2}$	$-\frac{3}{2}$	$\frac{3}{2}$	$-\frac{3}{2}$	$-\frac{3}{2}$	$\frac{3}{2}$	$-\frac{3}{2}$

Table I. Nodal coordinates in the (r, s) natural system for the three eigenmodes that constitute the "shear base"

Using the three sets of nodal coordinates displayed in Table I and the unstrained nodal coordinates $\left(r^k, s^k\right)$ we define three orthogonal nodal displacement vectors,

$$ {}^t\underline{\mathbf{\Psi}}_A^k = \left[\left({}^t\Phi_A^k\right)_r - r^k\right] \underline{\mathbf{e}}_r + \left[\left({}^t\Phi_A^k\right)_s - s^k\right] \underline{\mathbf{e}}_s. \tag{20} $$

In the above equation (r, s) are the isoparametric natural coordinate shown in Fig. 7; $(\underline{\mathbf{e}}_r; \underline{\mathbf{e}}_s)$ are orthonormal base vectors along those directions; the subindex $A = I...III$ indicates the deformation mode and the upper index $k = 1...4$ indicates the node.

For 4-node elements defined in the (x_1, x_2) coordinate system we generalize Eqn. (20) using the following extrapolation,

$$ {}^t\underline{\mathbf{\Psi}}_A^k = \left[h_j \left(\left({}^t\Phi_A^k\right)_r, \left({}^t\Phi_A^k\right)_s\right) \; x_i^j - x_i^k \right] \underline{\mathbf{e}}_i \tag{21} $$

where x_i^k is the $i-$coordinate of the $k-$node, the h_j are the isoparametric interpolation functions [5] and the index j indicates a summation from 1 to the number of nodes.

At any point inside the isoparametric element, the displacements corresponding to the *"shear base"* modes are interpolated as,

$$ {}^t\underline{\mathbf{\Psi}}_A = h_k \; {}^t\underline{\mathbf{\Psi}}_A^k. \tag{22} $$

We now compute, at the element center, the strain components resulting from the application of the three modes that we defined above,

$$ \underline{\boldsymbol{\varepsilon}}_I = \underline{\mathbf{B}}_c \underline{\mathbf{\Psi}}_I \tag{23a} $$

$$ \underline{\boldsymbol{\varepsilon}}_{II} = \underline{\mathbf{B}}_c \underline{\mathbf{\Psi}}_{II} \tag{23b} $$

$$ \underline{\boldsymbol{\varepsilon}}_{III} = \underline{\mathbf{B}}_c \underline{\mathbf{\Psi}}_{III} \tag{23c} $$

where $\underline{\mathbf{B}}_c = \underline{\mathbf{B}}(x_1^o, \; x_2^o)$ is the strain-displacements matrix calculated at the element center [2]. The linear combination of the above defined strain fields results in the shear band localization strains $\underline{\boldsymbol{\varepsilon}}_{sb}$, where β_I, β_{II} and β_{III} are constant parameters to be determined,

$$ \underline{\boldsymbol{\varepsilon}}_{sb} = \beta_I \underline{\boldsymbol{\varepsilon}}_I + \beta_{II} \underline{\boldsymbol{\varepsilon}}_{II} + \beta_{III} \underline{\boldsymbol{\varepsilon}}_{III} = \underline{\mathbf{B}}_c \left(\beta_I \underline{\mathbf{\Psi}}_I + \beta_{II} \underline{\mathbf{\Psi}}_{II} + \beta_{III} \underline{\mathbf{\Psi}}_{III}\right) \tag{24} $$

[2] It is important to realize that the volume change of a quadrilateral element can be exactly integrated using a one point Gauss quadrature (see Appendix).

To calculate β_I, β_{II} and β_{III}, we request that the strains $\underline{\boldsymbol{\varepsilon}}_{sb}$ fulfill incompressibility; hence, using Voight notation,

$$\begin{aligned} (\varepsilon_1+\varepsilon_2)_{sb} &= \beta_I\,(\varepsilon_1+\varepsilon_2)_I + \beta_{II}\,(\varepsilon_1+\varepsilon_2)_{II} + \beta_{III}\,(\varepsilon_1+\varepsilon_2)_{III} = 0 \quad (25a)\\ (\varepsilon_1+\varepsilon_2+\varepsilon_4)_{sb} &= \beta_I\,(\varepsilon_1+\varepsilon_2+\varepsilon_4)_I + \beta_{II}\,(\varepsilon_1+\varepsilon_2+\varepsilon_4)_{II} + \beta_{III}\,(\varepsilon_1+\varepsilon_2+\varepsilon_4)_{III} = 0 \quad (25b)\end{aligned}$$

where the first of the above equations corresponds to plane stress /plane strain cases while the second one to axisymmetric problems. We have one equation with three unknowns; therefore, we have to impose two constrains.

As a first constrain we adopt a value for β_{III}. If $\underline{\boldsymbol{\varepsilon}}_I$ and $\underline{\boldsymbol{\varepsilon}}_{II}$ are incompressible modes we adopt $\beta_{III} = 0$ since no volume correction is required to satisfy the incompressibility condition ; if not we adopt $\beta_{III} = 1$.

The second constrain is that the maximum distortion is localized at an angle α, defined by the shear band direction, hence,

$$\frac{(\varepsilon_3)_{sb}}{(\varepsilon_1-\varepsilon_2)_{sb}} = \frac{\beta_I\,(\varepsilon_3)_I + \beta_{II}\,(\varepsilon_3)_{II} + \beta_{III}\,(\varepsilon_3)_{III}}{\beta_I\,(\varepsilon_1-\varepsilon_2)_I + \beta_{II}\,(\varepsilon_1-\varepsilon_2)_{II} + \beta_{III}\,(\varepsilon_1-\varepsilon_2)_{III}} = \tan\left(2\alpha+\frac{\pi}{2}\right) \quad (26)$$

Solving the Eqns. (25a or 25b and 26) the parameters β_I and β_{II} are determined. Then we determine and normalize $\underline{\boldsymbol{\Theta}}$; from (24),

$$\underline{\boldsymbol{\Theta}} = \frac{\beta_I\underline{\boldsymbol{\Psi}}_I + \beta_{II}\underline{\boldsymbol{\Psi}}_{II} + \beta_{III}\underline{\boldsymbol{\Psi}}_{III}}{|\beta_I\underline{\boldsymbol{\Psi}}_I + \beta_{II}\underline{\boldsymbol{\Psi}}_{II} + \beta_{III}\underline{\boldsymbol{\Psi}}_{III}|}$$

We summarize by stating that the obtained localized displacement mode has maximum distortion along the shear band direction, no volume change and a norm $|\underline{\boldsymbol{\Theta}}| = 1$.

3.2 The element equilibrium equations

For the body shown in Fig. 8 , in equilibrium at time t, and considering that a shear band has already been triggered, we seek the equilibrium configuration for time $t+\Delta t$, via the principle of virtual work. For a "material nonlinear only analysis" (geometrically linear analysis) [5] we get, using the notation in Fig. 9,

$$\int_V \delta\,[\underline{\boldsymbol{\varepsilon}}_{cont}]^T\ {}^{t+\Delta t}\underline{\boldsymbol{\sigma}}_{cont}\,dv \;+\; \delta\,[\underline{\mathbf{U}}_{sb}]^T\ {}^{t+\Delta t}\underline{\mathbf{F}}_{sb} = \int_S \delta\underline{\mathbf{u}}^T\ {}^{t+\Delta t}\underline{\mathbf{p}}\,ds. \quad (27)$$

In the above equation,

$$\begin{aligned} V &= V_1 \cup V_2 \quad (28a)\\ S &= S_1 \cup S_2. \quad (28b)\\ {}^{t+\Delta t}\underline{\mathbf{p}} &= {}^{t+\Delta t}\underline{\mathbf{p}}_1 \cup {}^{t+\Delta t}\underline{\mathbf{p}}_2 \quad (28c)\end{aligned}$$

The vectors $\underline{\boldsymbol{\varepsilon}}_{cont}$ and ${}^{t+\Delta t}\underline{\boldsymbol{\sigma}}_{cont}$are related to the continuous scale while in the vector ${}^{t+\Delta t}\underline{\mathbf{F}}_{sb}$ we have the nodal forces generated by the shear band localization modes (localization scale).

Using Eqns. (18) and (19) we get for the continuous displacements,

$$\underline{\mathbf{u}}_{cont} = \underline{\mathbf{H}}\ (\underline{\mathbf{U}} - \gamma\underline{\mathbf{\Theta}}) \tag{29a}$$
$$\underline{\boldsymbol{\varepsilon}}_{cont} = \underline{\mathbf{B}}\ (\underline{\mathbf{U}} - \gamma\underline{\mathbf{\Theta}}) \tag{29b}$$

where $\underline{\mathbf{H}}$ is the displacements interpolation matrix, $\underline{\mathbf{B}}$ is the displacements-strains matrix, $\underline{\mathbf{U}}$ the nodal incremental displacements and γ the generalized displacement in the $\underline{\mathbf{\Theta}}$ direction.

Using the continuum constitutive relation we can write,

$$^{t+\Delta t}\underline{\boldsymbol{\sigma}}_{cont} = {}^{t}\underline{\boldsymbol{\sigma}}_{cont} + {}^{t}\left[\underline{\mathbf{C}}^{\mathbf{EP}}\right]\ \underline{\mathbf{B}}\ (\underline{\mathbf{U}} - \gamma\underline{\mathbf{\Theta}})\,. \tag{30}$$

It is necessary to establish the band forces evolution along an incremental step. To accomplish this we relate the continuum scale to the shear band scale via the plastic strains: we postulate that the incremental localized strains equal the incremental continuum strains produced by the localized displacement mode,

$$\underline{\boldsymbol{\varepsilon}}_{sb} = \underline{\mathbf{B}}\ \underline{\Theta}\ \gamma\ . \tag{31}$$

Hence, the relation between the incremental equivalent plastic deformation ($\bar{\varepsilon}$) and the localized strains is,

$$\bar{\varepsilon}^2 = \frac{2}{3}\,\varepsilon^P_{ij}\,\varepsilon^P_{ij} = \frac{2}{3}\,\underline{\boldsymbol{\varepsilon}}^T_{sb}\ \underbrace{\begin{bmatrix} 1 & 0 & 0 \\ 0 & 1 & 0 \\ 0 & 0 & \frac{1}{2} \end{bmatrix}}_{\underline{\mathbf{A}}}\ \underline{\boldsymbol{\varepsilon}}_{sb} = \frac{2}{3}\,\gamma\,\underline{\Theta}^T\,\underline{\mathbf{B}}^T\underline{\mathbf{A}}\,\underline{\mathbf{B}}\,\underline{\Theta}\,\gamma = \frac{2}{3}\,\varphi^2\gamma^2 \tag{32}$$

and,

$$^{t+\Delta t}\gamma = {}^{t}\gamma + \gamma \tag{33a}$$
$$^{t+\Delta t}\bar{\varepsilon} = {}^{t}\bar{\varepsilon} + \bar{\varepsilon} \tag{33b}$$

In the above equations,

- $\underline{\mathbf{A}}$ is the matrix required to preserve the dyadic tensorial product in Voight notation,
- for plane stress and plane strain elements $\underline{\boldsymbol{\varepsilon}}^T_{sb} = \left[(\varepsilon_{sb})_{xx} \quad (\varepsilon_{sb})_{yy} \quad 2\,(\varepsilon_{sb})_{xy}\right]$,
- for axisymmetric elements $\underline{\boldsymbol{\varepsilon}}^T_{sb} = \left[(\varepsilon_{sb})_{xx} \quad (\varepsilon_{sb})_{yy} \quad (\varepsilon_{sb})_{\theta\theta} \quad 2\,(\varepsilon_{sb})_{xy}\right]$,
- $\varphi^2 = \underline{\Theta}^T\,\underline{\mathbf{B}}^T\underline{\mathbf{A}}\,\underline{\mathbf{B}}\,\underline{\Theta}$ [3].

Hence,

$$\bar{\varepsilon} = \left[\sqrt{\frac{2}{3}}\,\varphi\right]\ \gamma\ . \tag{34}$$

[3] For axisymmetric problems $\underline{A}$ is a (4×4) matrix.

We impose that the band will only deform by sliding along its direction and that it will behave as a rigid-plastic solid when the sliding is increased. If unloading conditions arise the band will remain at its last plastic deformation stage and the continuous part of the model will produce the elastic unloading.

Since for each element where localization has taken place we keep the shear band direction constant, if the band is active the equation — $\det\left({}^{t}\hat{Q}_{jk}\right)=0$ — has to be fulfilled along all deformation stages; hence, from Eqn.(7), it is obvious that the stress tensor has to evolve radially if the band is active, therefore

$$ {}^{t+\Delta t}\sigma_{ij} = k\ {}^{t}\sigma_{ij} \tag{35a} $$

$$ k \geqslant 1\ . \tag{35b} $$

Since during the deformation process the material remains inside the plastic range, its yield stress has to evolve as,

$$ {}^{t+\Delta t}\sigma_{y} = k\ {}^{t}\sigma_{y}\ . \tag{36} $$

Equation (35a) and the fact that band direction is kept constant along the deformation process, imply that the equivalent nodal forces have to also evolve radially; hence,

$$ {}^{t+\Delta t}\underline{\mathbf{F}}_{sb} = k\ {}^{t}\underline{\mathbf{F}}_{sb} \tag{37} $$

therefore for a hardening material,

$$ \frac{\underline{\boldsymbol{\Theta}}^{T}\ {}^{t+\Delta t}\underline{\mathbf{F}}_{sb} - \underline{\boldsymbol{\Theta}}^{T}\ {}^{t}\underline{\mathbf{F}}_{sb}}{\underline{\boldsymbol{\Theta}}^{T}\ {}^{t}\underline{\mathbf{F}}_{sb}} = \frac{{}^{t+\Delta t}\sigma_{y} - {}^{t}\sigma_{y}}{{}^{t}\sigma_{y}} = \frac{{}^{t}H\ \left({}^{t+\Delta t}\bar{\varepsilon}\ -\ {}^{t}\bar{\varepsilon}\right)}{{}^{t}\sigma_{y}} = \frac{{}^{t}H\ \varphi\ \sqrt{\frac{2}{3}}\ \gamma}{{}^{t}\sigma_{y}} \tag{38} $$

where ${}^{t}H = \frac{\partial \sigma_{y}}{\partial \bar{\varepsilon}}$is the material hardening coefficient in the $t-$configuration.

For a bilinear material model, ${}^{t}H = (E\ E_{T})\ /\ (E - E_{T})$ [45]; where E is Young's modulus and E_{T} is the tangential plastic modulus.

From Eqn.(38) we get, for the nodal forces generated by the shear band localization modes, the evolution equation:

$$ \underline{\boldsymbol{\Theta}}^{T}\ {}^{t+\Delta t}\underline{\mathbf{F}}_{sb} = \underline{\boldsymbol{\Theta}}^{T}\ {}^{t}\underline{\mathbf{F}}_{sb}\ \left(1 + \frac{{}^{t}H\ \varphi\ \sqrt{\frac{2}{3}}\ \gamma}{{}^{t}\sigma_{y}}\right). \tag{39} $$

If the shear band opens at the $\tau-$configuration, we have as initial condition for Eqn.(39),

$$ \underline{\boldsymbol{\Theta}}^{T}\ {}^{\tau}\underline{\mathbf{F}}_{sb} = \underline{\boldsymbol{\Theta}}^{T}\ {}^{\tau}\underline{\mathbf{F}} = \underline{\boldsymbol{\Theta}}^{T} \int_{V} \mathbf{B}^{T}\ {}^{\tau}\boldsymbol{\sigma}\ dv \tag{40} $$

Since we have discussed above that there is no localization for hardening materials, Eqn.(39) is only valid for ${}^{t}E_{T} \leqslant 0$. For perfectly plastic materials we get, $\underline{\boldsymbol{\Theta}}^{T}\ {}^{t+\Delta t}\underline{\mathbf{F}}_{sb} = \underline{\boldsymbol{\Theta}}^{T}\ {}^{t}\underline{\mathbf{F}}$.

Using Eqns.(30) and (39) in (27) and solving for $\delta\underline{\mathbf{U}}$ and $\delta\underline{\gamma}$ we get

$$\delta\underline{\mathbf{U}}^T \left(\int_V \underline{\mathbf{B}}^{T\ t}\left[\underline{\mathbf{C}}^{\mathbf{EP}}\right]\ \underline{\mathbf{B}}\ (\underline{\mathbf{U}} - \gamma\underline{\mathbf{\Theta}})\ dv\ + \int_V \underline{\mathbf{B}}^{T\ t}\underline{\boldsymbol{\sigma}}_{cont}\ dv\ - \int_S \underline{\mathbf{H}}^{T\ t+\Delta t}\underline{\mathbf{p}}\ ds \right) = 0$$

$$\delta\underline{\gamma} \left(\int_V -\underline{\mathbf{\Theta}}^T\underline{\mathbf{B}}^T \left({}^t\underline{\boldsymbol{\sigma}}_{cont}\ +\ {}^t\left[\underline{\mathbf{C}}^{\mathbf{EP}}\right]\ \underline{\mathbf{B}}\ (\underline{\mathbf{U}} - \gamma\underline{\mathbf{\Theta}}) \right) dv\ +\ \underline{\mathbf{\Theta}}^{T\ t+\Delta t}\underline{\mathbf{F}}_{sb} \right) = 0$$

Since $\delta\underline{\mathbf{U}}$ and $\delta\underline{\gamma}$ are arbitrary we get,

$$\begin{bmatrix} {}^t\underline{\mathbf{K}}_u & -{}^t\underline{\mathbf{K}}_u\ \underline{\mathbf{\Theta}} \\ -\underline{\mathbf{\Theta}}^T\ {}^t\underline{\mathbf{K}}_u & \underline{\mathbf{\Theta}}^T\ {}^t\underline{\mathbf{K}}_u\ \underline{\mathbf{\Theta}} + \underline{\mathbf{\Theta}}^T\ {}^t\underline{\mathbf{F}}_{sb}\left(\frac{{}^tH\ \varphi\ \sqrt{\frac{2}{3}}}{{}^t\sigma_y}\right) \end{bmatrix} \begin{bmatrix} \underline{\mathbf{U}} \\ \underline{\gamma} \end{bmatrix} = \begin{bmatrix} {}^{t+\Delta t}\underline{\mathbf{R}} - {}^t\underline{\mathbf{F}} \\ \underline{\mathbf{\Theta}}^T\ ({}^t\underline{\mathbf{F}} - {}^t\underline{\mathbf{F}}_{sb}) \end{bmatrix} \tag{41}$$

where,

$${}^t\underline{\mathbf{K}}_u = \int_V \underline{\mathbf{B}}^{T\ t}\left[\underline{\mathbf{C}}^{EP}\right]\ \underline{\mathbf{B}}\ dv$$

$${}^{t+\Delta t}\underline{\mathbf{R}} = \int_S \underline{\mathbf{H}}^{T\ t+\Delta t}\underline{\mathbf{p}}\ ds$$

$${}^t\underline{\mathbf{F}} = \int_V \underline{\mathbf{B}}^{T\ t}\underline{\boldsymbol{\sigma}}\ dv$$

Since the above equations correspond to the linearized step we have to iterate for solving the incremental step; using Newton iterations we get for the $n-th$ iteration,

$$\begin{bmatrix} {}^{t+\Delta t}\underline{\mathbf{K}}_u^{(n-1)} & -{}^{t+\Delta t}\underline{\mathbf{K}}_u^{(n-1)}\ \underline{\mathbf{\Theta}} \\ -\underline{\mathbf{\Theta}}^T\ {}^{t+\Delta t}\underline{\mathbf{K}}_u^{(n-1)} & \underline{\mathbf{\Theta}}^T\ {}^{t+\Delta t}\underline{\mathbf{K}}_u^{(n-1)}\ \underline{\mathbf{\Theta}} + \underline{\mathbf{\Theta}}^T\ {}^t\underline{\mathbf{F}}_{sb}^{(n-1)}\left(\frac{{}^tH\ \varphi\ \sqrt{\frac{2}{3}}}{{}^t\sigma_y}\right) \end{bmatrix} \begin{bmatrix} \Delta\underline{\mathbf{U}}^{(n)} \\ \Delta\underline{\gamma}^{(n)} \end{bmatrix} =$$

$$\begin{bmatrix} {}^{t+\Delta t}\underline{\mathbf{R}} - {}^{t+\Delta t}\underline{\mathbf{F}}^{(n-1)} \\ \underline{\mathbf{\Theta}}^T\ \left({}^{t+\Delta t}\underline{\mathbf{F}}^{(n-1)} - {}^{t+\Delta t}\underline{\mathbf{F}}_{sb}^{(n-1)}\right) \end{bmatrix} \tag{42}$$

where,

$$\begin{aligned} {}^{t+\Delta t}\underline{\mathbf{K}}_u^{(n-1)} &= \int_V \underline{\mathbf{B}}^{T\ t+\Delta t}\left[\underline{\mathbf{C}}^{EP}\right]^{(n-1)}\ \underline{\mathbf{B}}\ dv \\ \underline{\mathbf{U}}^{(n)} &= \underline{\mathbf{U}}^{(n-1)} + \Delta\underline{\mathbf{U}}^{(n)} \\ \left[{}^{t+\Delta t}\underline{\gamma}\right]^{(n)} &= \left[{}^{t+\Delta t}\underline{\gamma}\right]^{(n-1)} + \Delta\underline{\gamma}^{(n)} \end{aligned}$$

The parameter $\Delta\underline{\gamma}$ is condensed at the element level and the resulting stiffness matrix is symmetric. It is important to highlight that the new formulation does not increment the number of d.o.f. as compared with the standard formulations; however, it requires a larger calculation effort.

4 Numerical implementation and some verification problems

4.1 Numerical implementation

For the implementation of our formulation we use several heuristic rules that we developed from our numerical experimentation:

- To detect the triggering of localization at an element, aside from tracking the plastic evolution at the standard Gauss points used to model the continuum response, we also track the plastic evolution at the element center. If at that point incremental plasticity is detected during a step iteration process [9], the band displacement mode is added to the element, i.e. localization is activated. As this mode is condensable, only the elements where localization was detected are affected by the formulation and the element band parameters $\underline{\gamma}$ are calculated via element decondensation.

- At every step all bands are deactivated and are afterwards activated during the iteration process if the localization condition is fulfilled. Since the bands are modeled using a rigid-plastic model, only growing bands will be active and the unloading of previously localized elements will be modeled by the continuous scale. If during a step iteration process, an element with an active band displacement mode does not develop incremental plasticity, the localization mode does not evolve at that time step ($\underline{\gamma} = 0$ and the tangent stiffness matrix does not incorporate the localization mechanism); hence, ${}^{t+\Delta t}\underline{\gamma} = {}^{t}\underline{\gamma}$.

- If during the iterations corresponding to an incremental step, an element alternatively develops incremental plasticity without localization (condition for localization mode activation) and does not develop incremental plasticity when the localization mode is activated (condition for localization mode deactivation) the algorithm cannot decide this bifurcation condition. To settle this decision, if this occurs more than a number of times during a step, the element is enforced to remain with the localization mode inactive, taking the non-localized branch of the bifurcation. Typical limiting values are for example $8 - 10$ activating-deactivating cycles.

- Band directions are determined according to the acoustic tensor conditions (9, 10) and are kept constant throughout the analysis. At this stage we have to select between two alternative directions and this is, as far as we know, a point still open in the literature. Following [39] for the first shear band that is triggered in the model we select one of the two directions and for the other ones we use a "persistence criterion", which means that in any new band we choose from the two possible directions, the one closer to the localization direction in the surrounding elements.

4.2 Verification problems: elastic / perfectly plastic material model

To test the new formulation we develop simple bidimensional test cases using $J2$ plasticity. In the following examples we consider a material with $E = 200GPa$, $\nu = 0.3$, ${}^{t}\sigma_y = 600MPa$, and a tangent plastic modulus $E_T = 0$.

In particular we analyze problems were the shear bands can fully develop and almost all the deformation energy concentrates in the band. We observe the behavior of the energy dissipated at the continuum scale, which is expected to decrease when the mesh is refined, and of the energy dissipated at the shear band scale, which is expected to converge when the mesh is refined.

4.2.1 Simple traction of a rectangular sheet

The problem under analysis is represented in Fig. 10. The first localization is induced by a reduction of 50% in the yield stress of the corner element.

We analyzed plane stress and strain cases using the following regular meshes:

Mesh	Horizontal Elem.	Vertical Elem.	Total Elem.
1	8	12	96
2	16	24	384
3	32	48	1536

Table II. Regular meshes used to analyze the simple traction of a rectangular sheet

In Figs. 11-12 we present the convergence studies for plane stress and plane strain conditions using undistorted elements. In those figures we show: the resulting load-displacement diagrams which display an excellent convergence when the mesh is refined without showing any mesh dependency; the total dissipated energy which remains almost unchanged with mesh refinement; the plastic energy dissipated by the continuum, which as expected decreases when the mesh is refined and the plastic energy dissipated by the localization modes, which as expected increases when the mesh is refined.

In Fig. 13 (plane stress) and Fig. 14 (plane strain) for the (16×24) mesh we compare the results obtained using undistorted and distorted elements. The results are quite independent of the mesh and we can only comment that the band width increases slightly and the band equivalent plastic strain distribution is slightly more diffused for the distorted mesh that for the undistorted one.

In order to visualize the difference between using standard element formulations and our new formulation enhanced with localization modes, in Figs. 15 to 17 we present some comparisons for the plane strain case at the step of maximum elongation.

In Fig. 15 we see that the high plastic deformations area in the continuum is much more extended when using the standard finite element formulations. In the best case (QMITC formulation) the plastic deformation is constrained to the size of one element.

In Fig. 16 we see the total equivalent plastic strain distribution for the different formulations. In the models that were developed using the standard Q1-P0 and Q2-P1 elements the shear band is not properly localized; in the model developed using the standard QMITC element the shear band localizes in one element but as the mesh is refined the value of the total equivalent plastic strain grows unbounded. In the case of our new formulation the equivalent plastic strain is localized in two small areas enclosing the band and does not present an unbounded growth with mesh refinement.

In Fig. 17 we analyze the relative lateral displacement between points A and B. We see that the standard formulations wrongly predict a vanishing horizontal displacement when the mesh is refined, while in the formulation enhanced with localization modes the horizontal displacement prediction converges fast to the definitive value and is not affected by the mesh refinement.

A similar problem was analyzed in [48] using a Cosserat continuum model and the results show "reduced mesh sensitivity". The Cosserat model includes a softening plastic behavior and other additional material parameters.

4.2.2 Simple shear

To analyze the behavior of our new formulation in varying mesh orientation cases, we test two square meshes of (9×9) elements in the two shear cases shown in Fig. 18: case (a) with shear bands developing diagonal

to the mesh and case (b) with shear bands developing aligned to the mesh. Localization is induced by a 50% yield stress reduction at the central element. The comparisons between the standard QMITC formulation and the QMITC enhanced with localization modes are shown in Figs. 19 and 20. In the case of the new formulation, the results obtained for the "aligned" case are better than the results obtained for the "diagonal" case. This worst behavior in the "diagonal case" may be attributed to the boundary effect at the corners, where the restrains prevent the development of the localization scale.

4.2.3 Indentation of a plane strain specimen

In Fig. 21 we present the results that we obtained when analyzing the indentation of a plane strain specimen using a 384 elements mesh; it is obvious that the energy is mostly dissipated by the localization modes. It can be seen that close to the band initiation point, the continuum has a significant plastic deformation, while along the band path almost all the plastic deformation is developed in the band, leaving the continuum scale plastically unstrained.

In Fig. 22 we present a convergence study for this problem where it is seen that the numerical results converge as we refine the mesh.

4.3 Verification problems: softening material model

Even though we do not use softening material models to simulate the structural softening, in the literature many researchers resort to this type of material models. In this example we show that in these cases our formulation is also able to provide mesh independent results.

Let us consider a material with $E_T = -E/10^2$; that is to say a material with a softening plastic behavior. We also use $E = 200GPa$, $\nu = 0.3$ and ${}^o\sigma_y = 600MPa$.

In Fig. 23 we present, for the simple traction of a plane strain rectangular sheet, the results obtained using the standard QMITC element formulation and the element enhanced with localization modes. As expected the standard formulation provides a very mesh dependent post-yielding result; however, the result produced by our new formulation is quite mesh independent.

5 Conclusions

In this paper we developed a new two-scale finite element formulation for modeling J_2 plastic deformation processes in which shear band localizations take place ($2D$).

The new formulation is based on the use of embedded strong discontinuity modes which are triggered using a stress based criterion. The basic finite element formulation, i.e. the QMITC element, that is enhanced with the embedded localization modes, was selected so as to prevent a spurious diffusion of the localized plastic deformations.

Considering the actual implementation of our new formulation it is important to point out that the order of the Gauss integration used for calculating the element stiffness and equivalent nodal forces equals the integration order used in standard finite element formulations and that the our two-scale formulation does not introduce extra d.o.f. in the assembled numerical model.

There are several advantages in our new formulation:

- It does not require the definition of non-physical strain softening stress/strain relations and does not use material properties like fracture energy, which have not been defined nor measured in the environment of J_2 plasticity.
- It does not require a specific mesh refinement to model the localization phenomena.
- It provides mesh independent results even if a softening stress/strain relation is used.
- Its results are quite insensitive to element distortions.

Acknowledgement 1 *We gratefully acknowledge the support of TENARIS for this research.*

A Quadrilateral elements: volume variation

The Jacobian for an isoparametric transformation is:

$$J = \begin{bmatrix} \frac{\partial x}{\partial r} & \frac{\partial y}{\partial r} \\ \frac{\partial x}{\partial s} & \frac{\partial y}{\partial s} \end{bmatrix} \; ; \; J^{-1} = \begin{bmatrix} \frac{\partial r}{\partial x} & \frac{\partial s}{\partial x} \\ \frac{\partial r}{\partial y} & \frac{\partial s}{\partial y} \end{bmatrix} = \frac{1}{|J|} \begin{bmatrix} \frac{\partial y}{\partial s} & -\frac{\partial y}{\partial r} \\ -\frac{\partial x}{\partial s} & \frac{\partial x}{\partial r} \end{bmatrix} \tag{A.1}$$

The volume change is:

$$\Delta V = \int_{-1}^{1}\int_{-1}^{1} \varepsilon_v \; |J| \; dr \; ds = \int_{-1}^{1}\int_{-1}^{1} \left(\frac{\partial u}{\partial x} + \frac{\partial v}{\partial y}\right) \; |J| \; dr \; ds =$$

$$\int_{-1}^{1}\int_{-1}^{1} \left(\frac{\partial u}{\partial r}\frac{\partial r}{\partial x} + \frac{\partial u}{\partial s}\frac{\partial s}{\partial x} + \frac{\partial v}{\partial r}\frac{\partial r}{\partial y} + \frac{\partial v}{\partial s}\frac{\partial s}{\partial y}\right) \; |J| \; dr \; ds \tag{A.2}$$

Replacing A.1 into A.2

$$\Delta V = \int_{-1}^{1}\int_{-1}^{1} \left(\frac{\partial u}{\partial r}\frac{1}{|J|}\frac{\partial y}{\partial s} - \frac{\partial u}{\partial s}\frac{1}{|J|}\frac{\partial y}{\partial r} - \frac{\partial v}{\partial r}\frac{1}{|J|}\frac{\partial x}{\partial s} + \frac{\partial v}{\partial s}\frac{1}{|J|}\frac{\partial x}{\partial r}\right) \; |J| \; dr \; ds$$

$$\Delta V = \int_{-1}^{1}\int_{-1}^{1} \left(\frac{\partial u}{\partial r}\frac{\partial y}{\partial s} - \frac{\partial u}{\partial s}\frac{\partial y}{\partial r} - \frac{\partial v}{\partial r}\frac{\partial x}{\partial s} + \frac{\partial v}{\partial s}\frac{\partial x}{\partial r}\right) \; dr \; ds$$

Simplifying

$$\Delta V = \int_{-1}^{1}\int_{-1}^{1} \left(h^k_{,r} \; u_k \; h^j_{,s} \; y_j - h^k_{,s} \; u_k \; h^j_{,r} \; y_j - h^k_{,r} \; v_k \; h^j_{,s} \; x_j + h^k_{,s} \; v_k \; h^j_{,r} \; x_j\right) \; dr \; ds \qquad\qquad j,k = 1..4$$

As all the terms have a product $h^k_{,r} \; h^j_{,s} \; \forall j,k$, the polynomial terms will be of order 1, r, s and rs. All those terms are exactly integrated using a one point Gauss quadrature; hence,

$$\Delta V \; = 4 \; \varepsilon_v|_{r=0 \; s=0} \; |J|_{r=0 \; s=0}$$

References

[1] W.A. Backofen, *Deformation Processing*, Addison-Weley, 1972.

[2] G.E. Dieter, *Mechanical Metallurgy*, McGraw-Hill, 1986.

[3] R. Dormeval, "The adiababtic shear phenomenon", in *Materials at High Strain Rates*, (Ed. T.Z. Blazynski), Elsevier, 1987.

[4] A. Needleman, "Dynamic shear band development in plane strain", *J. Appl. Mechs. ASME,* **56,** pp.1-9, 1989.

[5] K.J. Bathe, *Finite Element Procedures*, Prentice Hall, NJ, 1996.

[6] E.N.Dvorkin and S.I.Vassolo, "A quadrilateral 2D finite element based on mixed interpolation of tensorial components", *Engng. Computations*, **6**, pp.217-224, 1989.

[7] E.N.Dvorkin, A.P.Assanelli and R.G.Toscano, "Performance of the QMITC element in 2D elasto-plastic analyses", *Computers & Structures*, **58**, pp.1099-1129, 1996.

[8] P. Steinmann and K. Willam, "Performance of Enhanced Finite Element Formulations in Localized Failure Computations", *Comp. Meth. Appl. Mech. Engng.*, **90**, pp.845-867, 1991.

[9] M. Ortiz, Y. Leroy, A. Needleman, "A Finite-Element Method for Localized Failure Analysis", *Comput. Meth. Appl. Mechs. Engng.*, **61**, pp.189-214, 1987.

[10] E.N.Dvorkin, A.M.Cuitiño and G.Gioia, "Finite elements with displacement interpolated embedded localization lines insensitive to mesh size and distortions", *Int. J. Numerical Methods in Engng.*,**30**, pp.541-564, 1990.

[11] E.N.Dvorkin and A.P.Assanelli, "2D finite elements with displacement interpolated embedded localization lines: the analysis of fracture in frictional materials", *Comput. Meth. Appl. Mechs. Engng.*, **90**, pp.829-844, 1991.

[12] Z.P. Bažant, "Instability, ductility and size effect in starin softening concrete", *J. Eng. Mech. Div. ASCE*, **102**, 331-344 (1976); discussions, **103**, 357-358, 775-777 (1976); **104,** 501-502, (1976).

[13] N.S. Ottosen, "Thermodynamic consequences of strain softening in tension", *J. Eng. Mech. ASCE*, **112**, 1152-1164, 1986.

[14] J.G. van Mier, "Strain Softening of Concrete under Multiaxial Loading Conditions", *Doctoral Thesis*, Eindhoven Univ. of Tech., The Netherlands, 1984.

[15] P.A. Vermeer and R. de Borst, *Non-Associated Plasticity for Soils, Concrete and Rock*, Heron, 1984.

[16] Z.P. Bažant, "Size effect in blunt fracture: concrete, rock and metal", *J. Eng. Mechs. ASCE*, **110**, pp.518-534, 1984.

[17] R. de Borst and P. Nauta, "Non-orthogonal cracks in a smeared finite element model", *Engng. Computations*, **2**, pp.35-46, 1985.

[18] Z.P. Bažant, "Mechanics of distributed cracking", *Appl. Mechs. Rev. ASME*, **39,** pp.675-705, 1986.

[19] Z.P. Bažant and P.A. Pfeiffer, "Determination of fracture energy from size effect and brittle number", *ACI Mat. J.,* **84**, pp.463-480, 1987.

[20] M. Jirásek, "Comparative study on finite elements with embedded discontinuities", *Comput. Meth. Appl. Mechs. Engng.*, **188**, pp.307-330, 2000.

[21] Y.R. Rashid, "Analysis of prestressed concrete pressure vessels", *Nuclear Eng. Des.*, **7,** pp.334-355, 1968.

[22] Z.P. Bažant and B.H. Oh, "Crack band theory for fracture of concrete", *RILEM Mater. Struct.*, **16**, pp.155-177, 1983.

[23] Z.P. Bažant and B.H. Oh, "Rock fracture via strain softening finite elements", *J. Eng. Mechs. ASCE*, **110**, pp. 1015-1035, 1984.

[24] J. Oliver, "A consistent characteristic length for smeared cracking models", *Int. J. Numerical Methods in Engng.*, **28**, pp.461-474, 1989.

[25] A. Hilleborg, M. Modéer and P.E. Petersson, "Analysis of crack formation and crack growth in concrete by means of fracture mechanics and finite elements", *Cement Concr. Res.*, **6**, pp.773-782, 1976.

[26] A.R. Ingraffea and V. Saouma, "Numerical modeling of discrete crack propagation in reinforced and plane concrete", in *Fracture Mechanics of Concrete: Structural Application and Numerical calculation* (Eds. G.C. Sih and A. Tommaso), Martinus Nijhoff, Dordrech - The Netherlands, 1985.

[27] T. Belytschko, J. Fish and E. Engelman, "A finite element with embedded localization zones", *Comput. Meth. Appl. Mechs. Engng.*, **70**, pp.59-89, 1988.

[28] J. Oliver, "Modeling strong discontinuities in solid mechanics via strain softening constitutive equations. Part 1: Fundamentals", *Int. J. Numerical Methods in Engng.*, **39**, pp.3575-3600, 1996.

[29] J. Oliver, "Modeling strong discontinuities in solid mechanics via strain softening constitutive equations. Part 2: Numerical simulation", *Int. J. Numerical Methods in Engng.*, **39,** pp.3601-3623, 1996.

[30] R. de Borst and L.J. Sluys, "Localisation in a Cosserat continuum under static and dynamic loading conditions", *Comput. Meth. Appl. Mechs. Engng.*, **90**, pp.825-827, 1991.

[31] R. de Borst, L.J. Sluys, H.-B. Muhlhaus andJ. Pamin, "Fundamental issues in finite element analyses of localisation of deformation", *Engng. Computations,* **10**, pp.99-121, 1993.

[32] J. R. Rice, "The Localization of Plastic Deformation", in *Theoretical and Applied Mechanics* (Proceedings of the 14th International Congress on Theoretical and Applied Mechanics, Delft, 1976, ed. W.T. Koiter), Vol. 1, North-Holland Publishing Co., pp.207-220, 1976.

[33] N.S. Ottosen, K. Runesson, "Properties of discontinuous bifurcation solutions in elasto-plasticity". *Int. J. Solids Structures*, **27**, 401-421, 1991.

[34] R. Larsson, K. Runesson, N.S. Ottosen, "Discontinuous displacement approximation for capturing plastic localization", *Int. J. Num. Methods in Engng.,* **36**, 2087-2105, 1993.

[35] F. Armero and K. Garikipati, "Recent Advances in the Analysis and Numerical Simulation of Strain Localization in Inelastic Solids", *Proc. Computational Plasticity COMPLAS IV*, (Ed. by D.R.J Owen, E. Oñate and E. Hinton), Barcelona, 1995.

[36] F. Armero and K. Garikipati, "Analysis of Strong Discontinuities in Multiplicative Finite Strain Plasticity and Their Relation with the Numerical Simulation of Strain Localization in Solids", *Int. J. Solids and Structures*, **33**, pp.2863-2885, 1996.

[37] L.J. Sluys, "Discontinuous modeling of shear banding"In:Owen D J R,Onate E,Hinton E,eds.Computational Plasticity:Fundamentals and Applications,*Proc. Computational Plasticity COMPLAS V*, (Ed. by D.R.J Owen, E. Oñate and E. Hinton), Barcelona, 1997.

[38] N. Moës, J. Dolbow and T. Belytschko, "A Finite Element Method for Crack Growth Without Remeshing," *Int. J. Numerical Methods in Engng.*, **46**, pp. 131-150, 1999.

[39] E. Samaniego, T. Belytschko, "Continuum–discontinuum modelling of shear bands", *Int. J. Num. Methods in Engng.*,**62**, 1857-1872, 2005.

[40] P.M.A. Areias and T. Belytschko, "Two-scale shear band evolution by local partition of unity", *Int. J. Numerical Methods in Engng.*, **66**, pp.878-910, 2006.

[41] A. Hansbo and P. Hansbo,"An unfitted finite element method, based on Nitsche's method, for elliptic interface problems", *Comput. Meth. Appl. Mechs. Engng.,* **191**, pp.5537-5552, 2002.

[42] A. Hansbo and P. Hansbo, "A Finite Element method for the simulation of strong and weak discontinuities in elasticity", *Comput. Methods Appl. Mech. Engrg.,* **193**, pp. 3523–3540, 2004.

[43] J. Mergheim, E. Kuhl and P. Steinmann, "A finite element method for the computaitonal modelling of cohesive cracks", *Int. J. Numerical Methods in Engng*, **63**, pp.276-289, 2005.

[44] J. Mergheim, E. Kuhl, P. Steinmann, "Towards the algorithmic treatment of 3D strong discontinuities", *Communications in Numerical Methods in Engineering*, **23**, pp.97-108, 2007.

[45] E.N. Dvorkin and M.B. Goldschmit, *Nonlinear Continua*, Springer, Berlin, 2005.

[46] J. C. Simo and T.J.R. Hughes, *Computational Inelasticity*, Springer, 1997.

[47] R. Hill, *The Mathematical Theory of Plasticity*, Oxford at the Clarendon Press, 1983.

[48] E.N. Lages, G.H. Paulino, I.F.M. Menezes and R.R. Silva, "Nonlinear finite element analysis using an object-oriented philosophy - Application to beam elements and to Cosserat conrinuum", *Engineering with Computers*, **15**, pp.73-89, 1999.

Figure Captions:

1. Plane strain problem modeled using different finite element formulations
2. Shear band in the coupling of a threaded connection: QMITC results
3. Shear band in the coupling of a threaded connection: etched sample
4. Strategies for modeling localization phenomena
5. Vectors ${}^t\underline{\mathbf{m}}$ and ${}^t\underline{\mathbf{n}}$ defined for the shear band (mode II)
6. Volume change for a square element: zero for a sliding line parallel to the element sides and non-zero for a slanted sliding line
7. Eigenmodes that form the "shear base" (in solid lines we show the undistorted 2×2 element and in dotted lines the deformed element)
8. Solid with localized shear band
9. Equilibrium of a solid with a localization line
10. Rectangular sheet in simple traction
11. Rectangular sheet in simple traction - Plane stress. Convergence studies
12. Rectangular sheet in simple traction - Plane strain. Convergence studies
13. Rectangular sheet in simple tension - Plane stress. Effect of elements distortion
14. Rectangular sheet in simple tension - Plane strain. Effect of elements distortion
15. Comparison between the new formulation and standard element formulations. Continuum equivalent plastic deformation in plane strain
16. Comparison between the new formulation and standard element formulations. Continuum equivalent plastic strain in a section normal to the shear band
17. Comparison between the new formulation and standard element formulations. Relative horizontal displacement between points A and B
18. Shear cases analyzed
19. Localization in simple shear using the standard QMITC element and the QMITC element enhanced with localization modes
20. Energy dissipation in simple shear. QMITC element vs. QMITC element enhanced with localization modes
21. Indentation of a plane strain specimen: displacements and plastic strains
22. Indentation of a plane strain specimen: convergence analysis

23. Softening material model. Plane strain rectangular sheet in simple traction

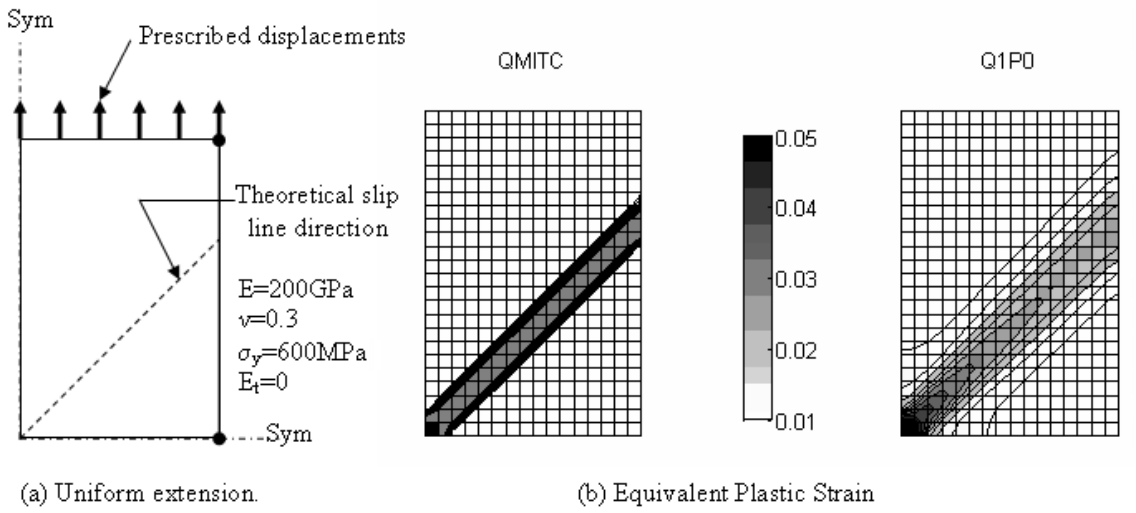

Figure 1

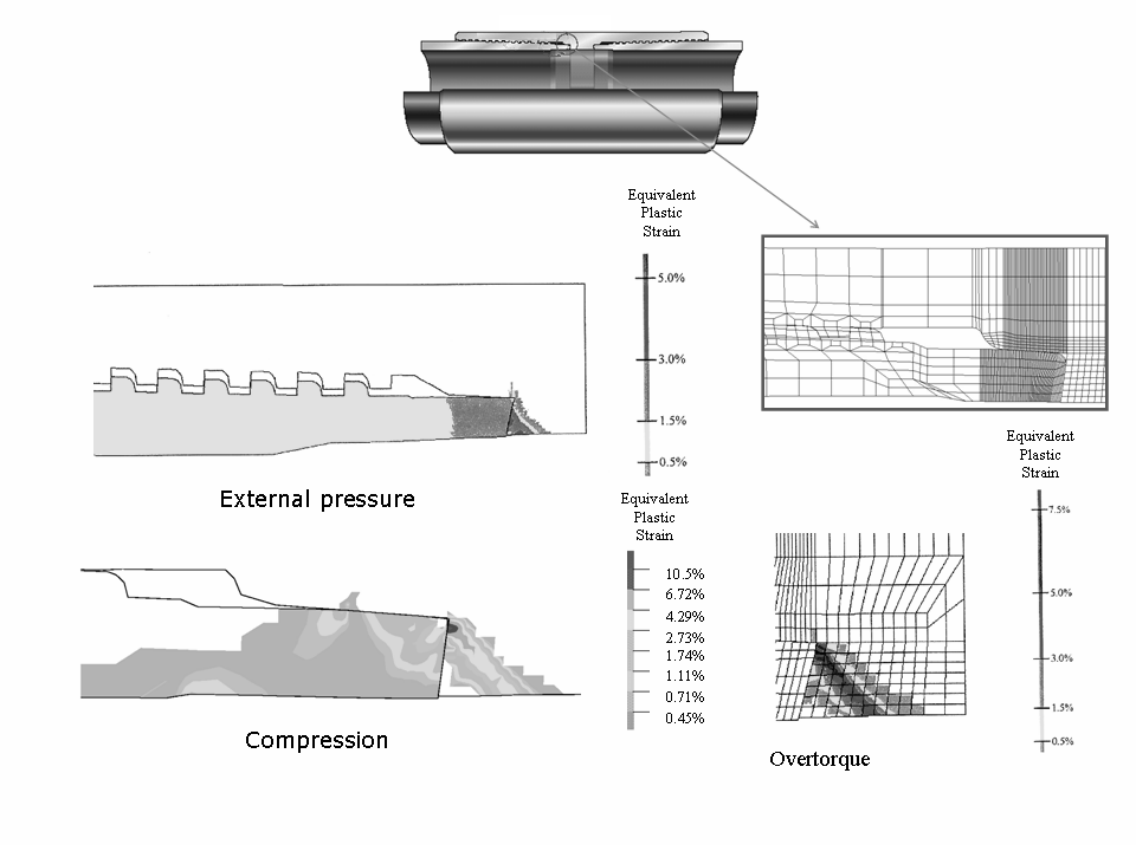

Figure 2

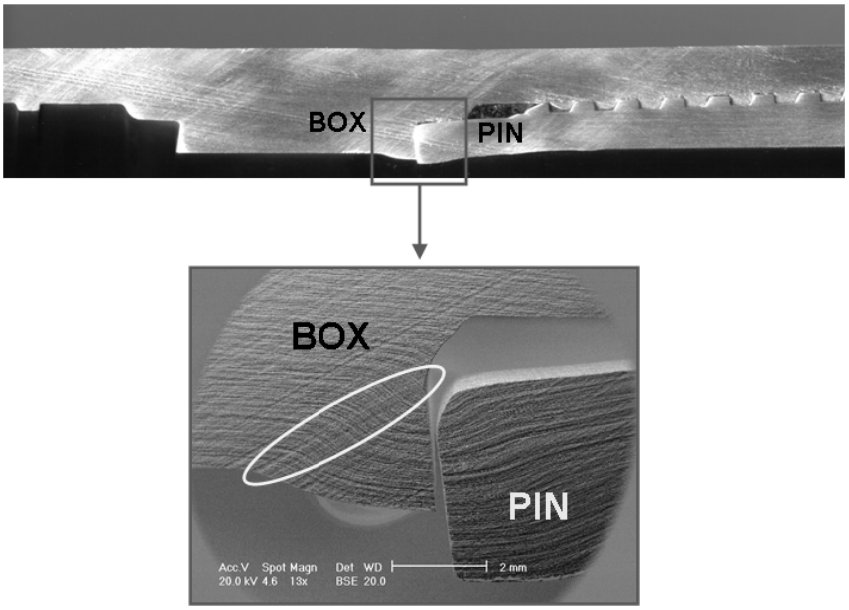

Figure 3

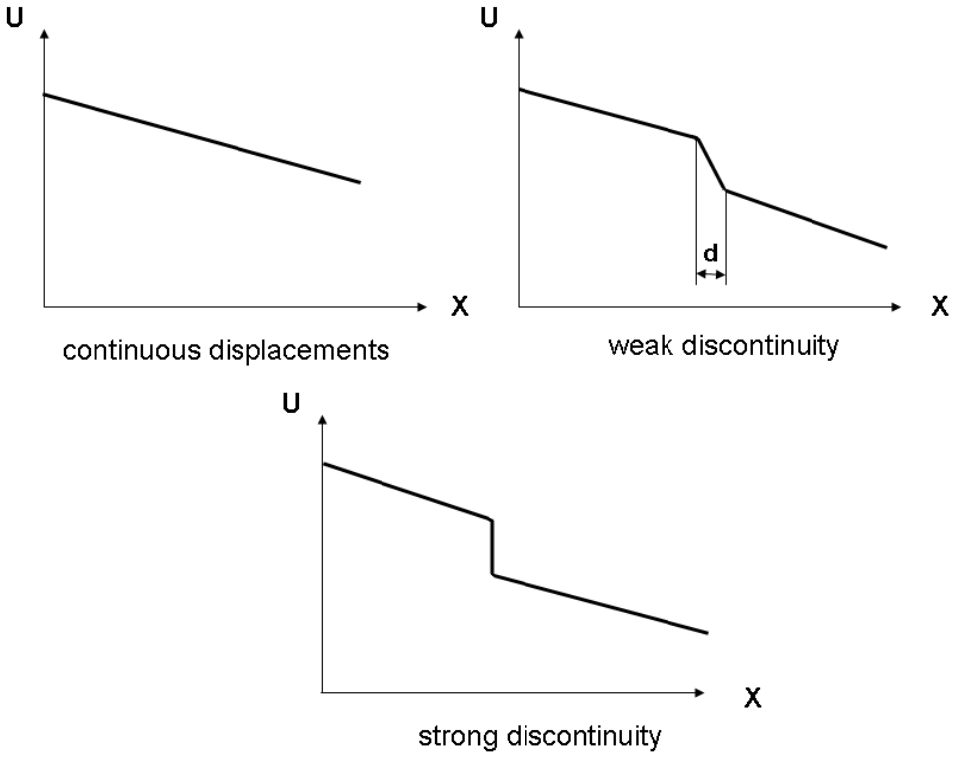

Figure 4

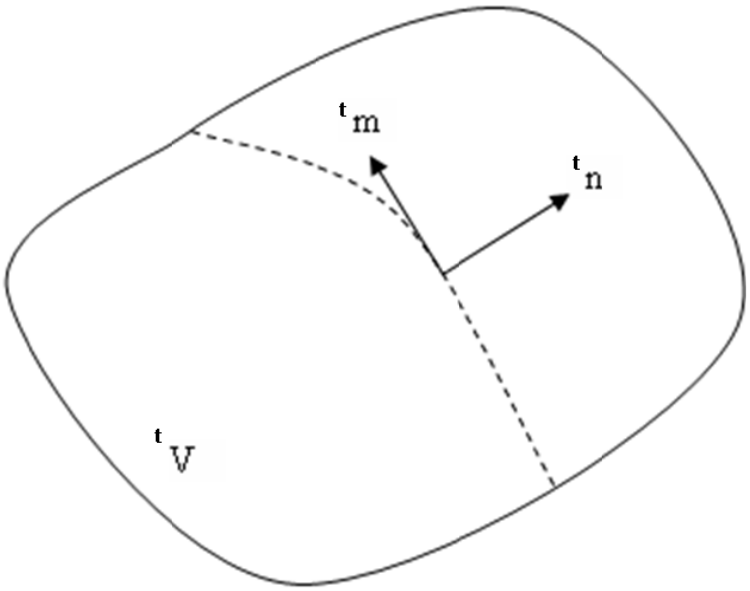

Figure 5

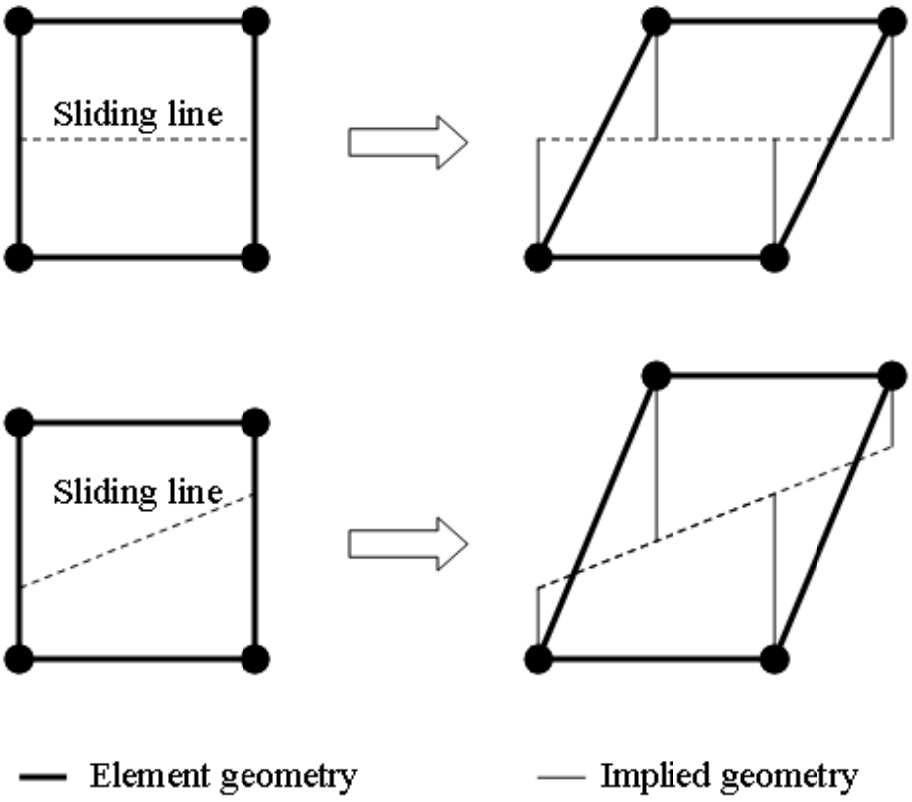

Figure 6

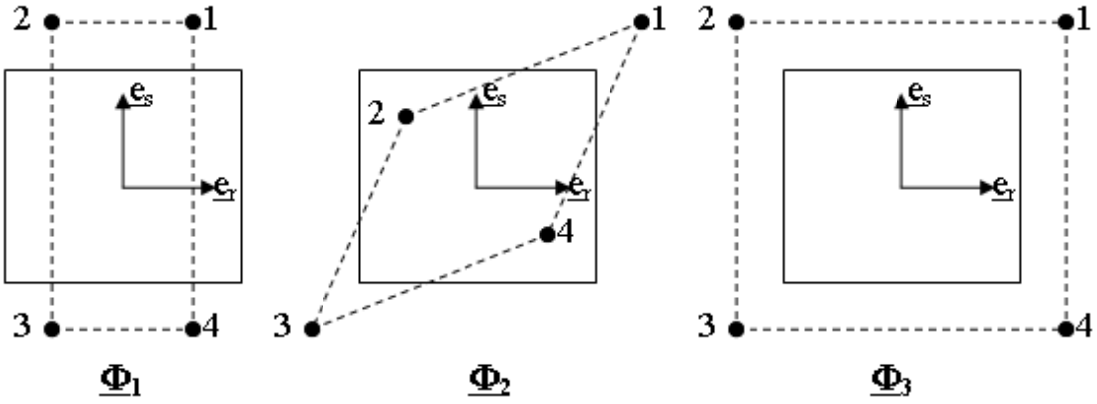

Figure 7

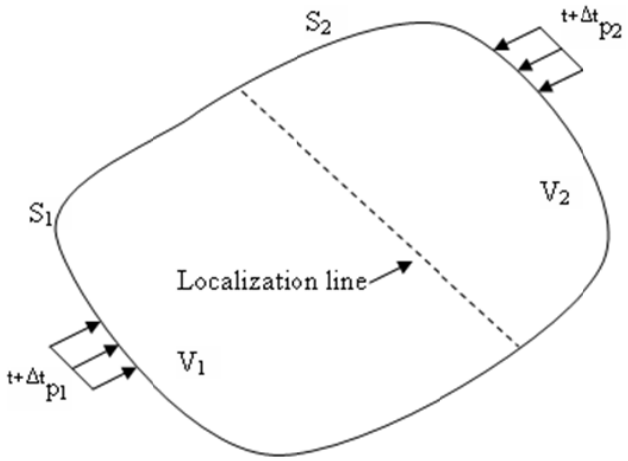

Figure 8

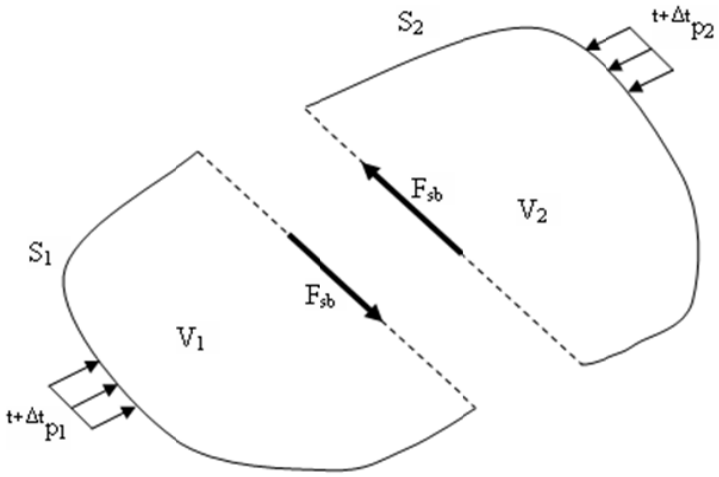

Figure 9

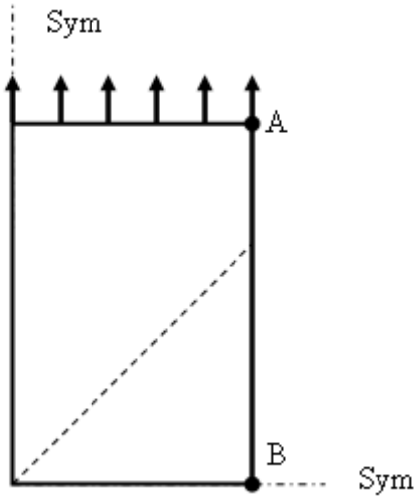

Figure 10

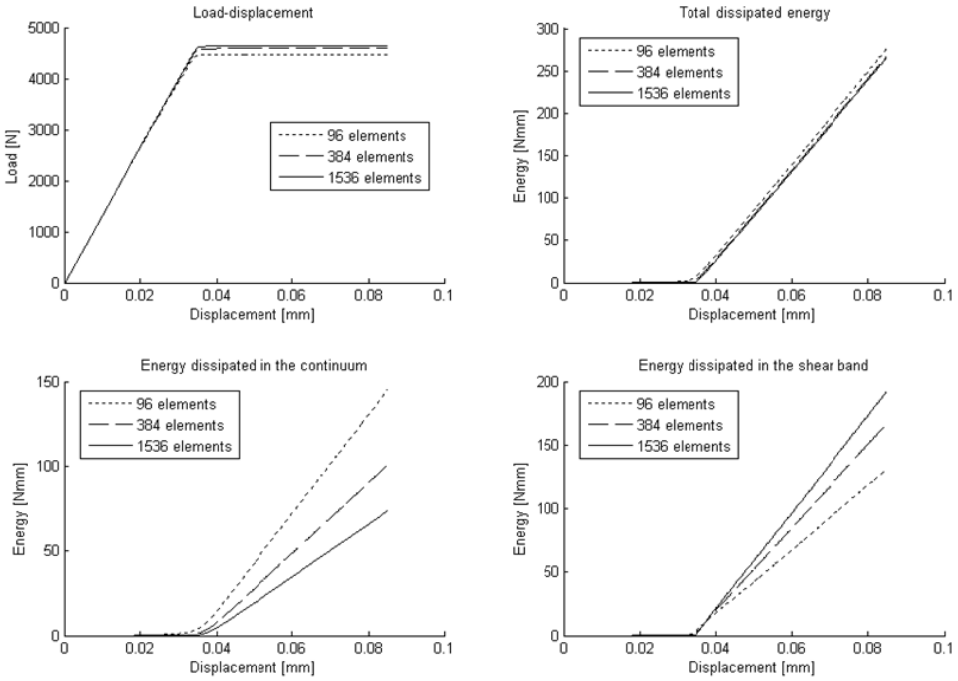

Figure 11

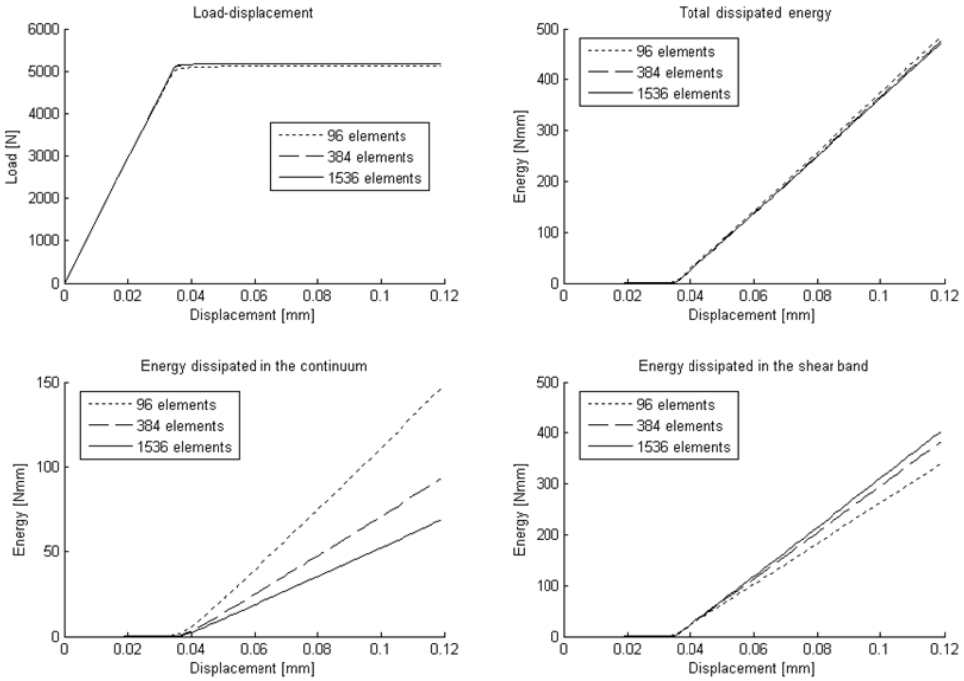

Figure 12

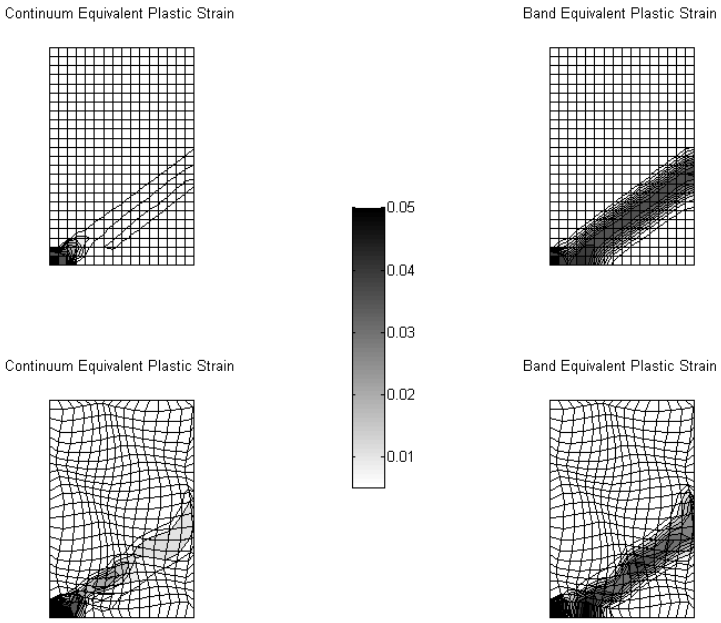

Figure 13

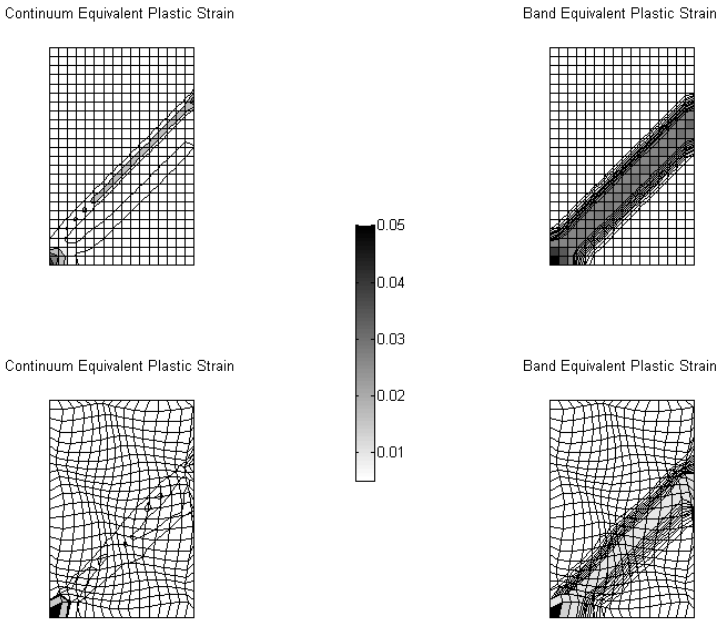

Figure 14

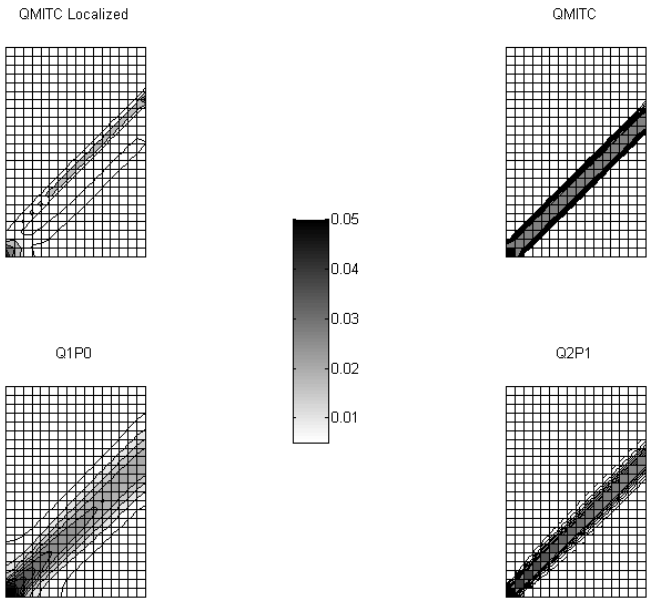

Figure 15

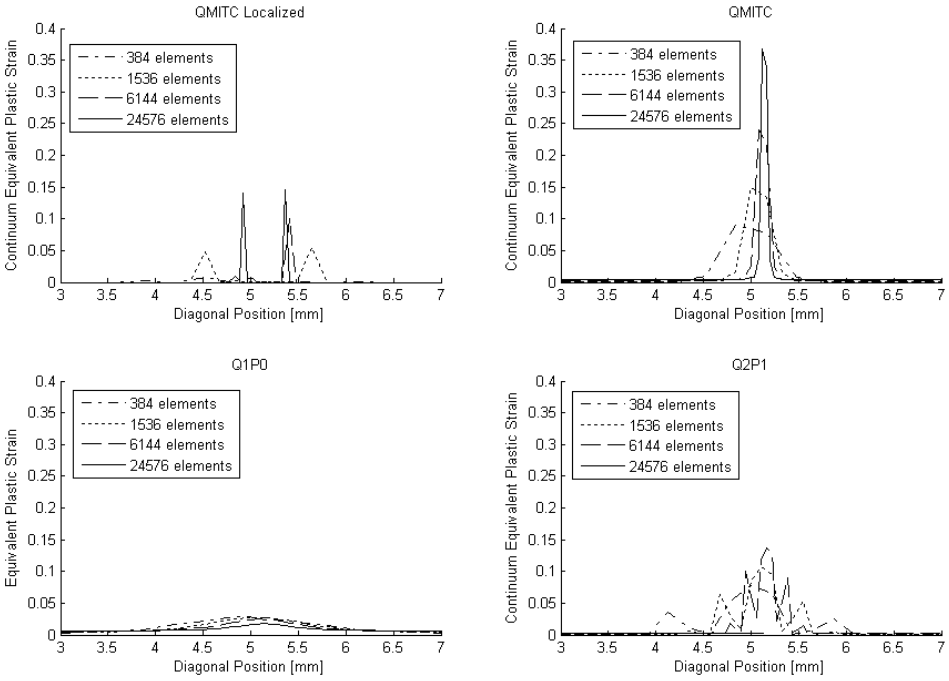

Figure 16

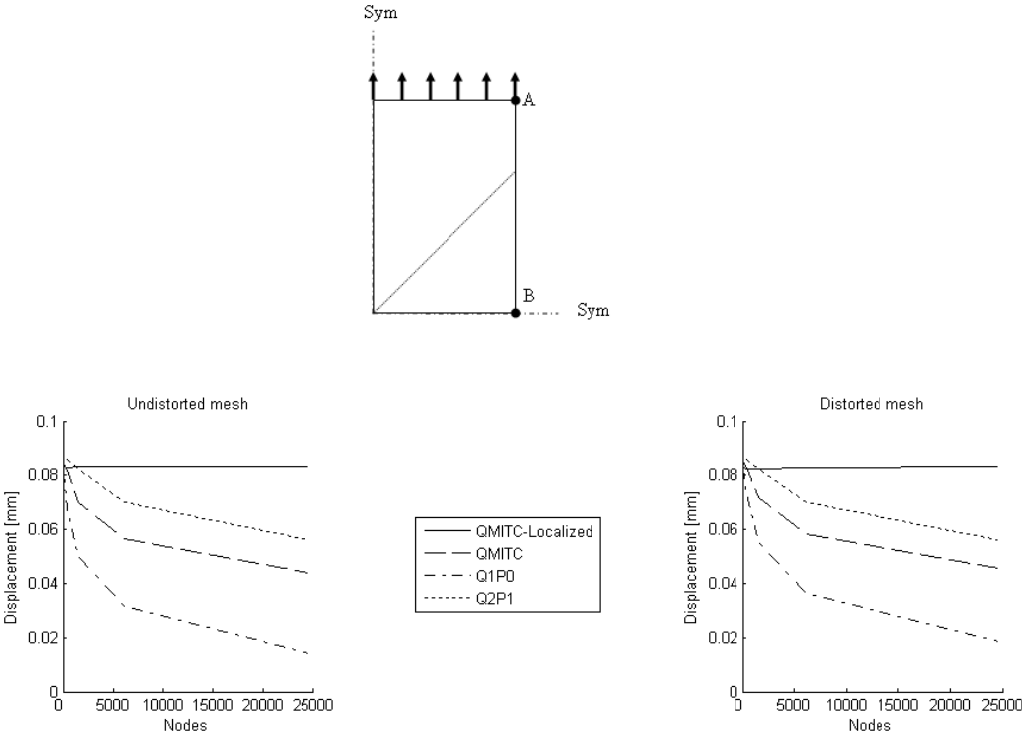

Figure 17

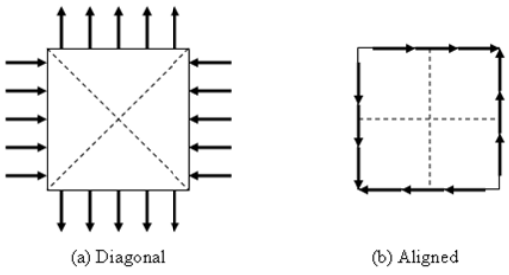

Figure 18

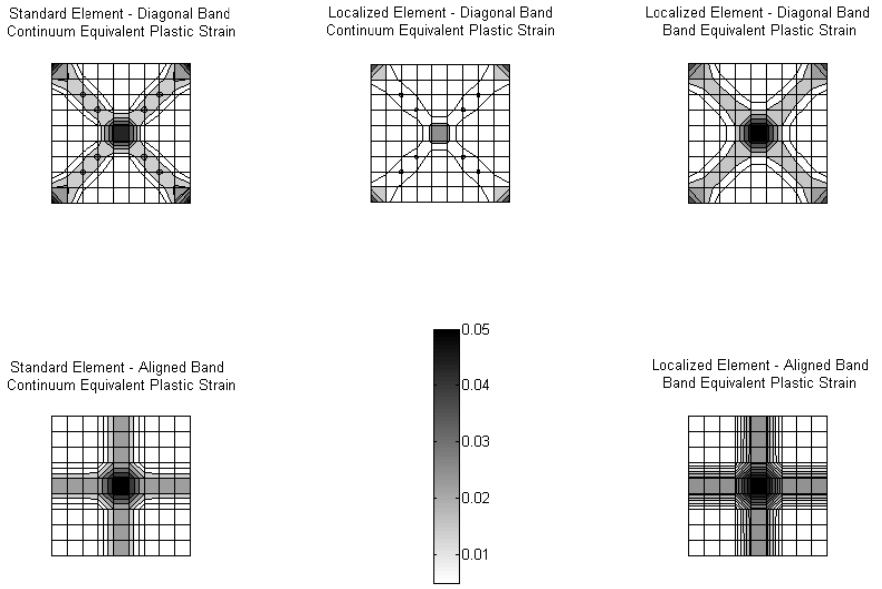

Figure 19

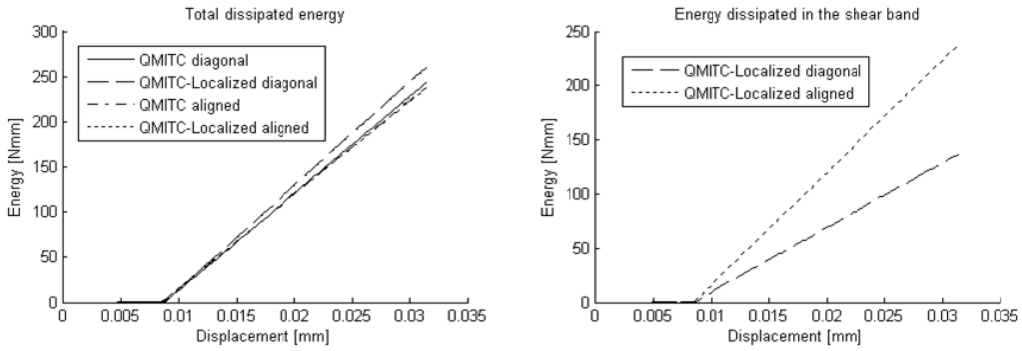

Figure 20

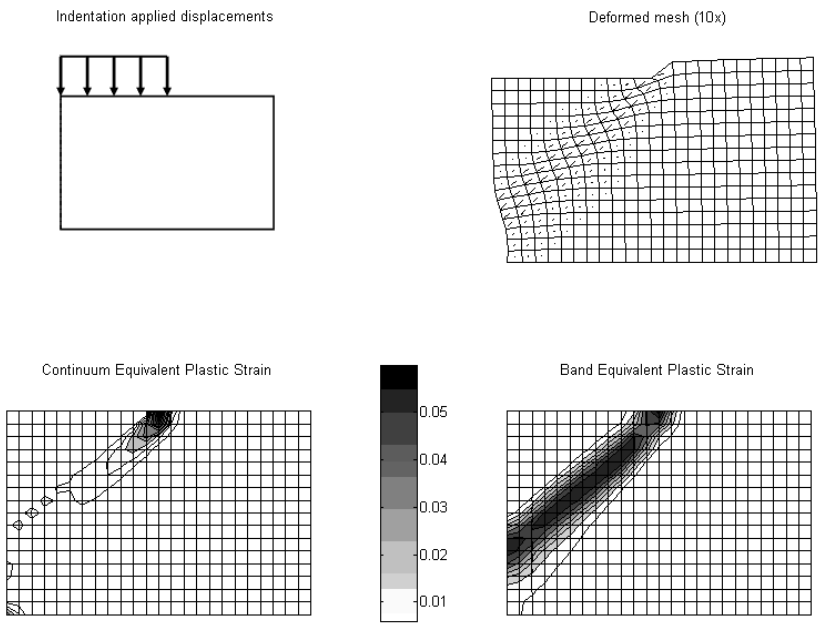

Figure 21

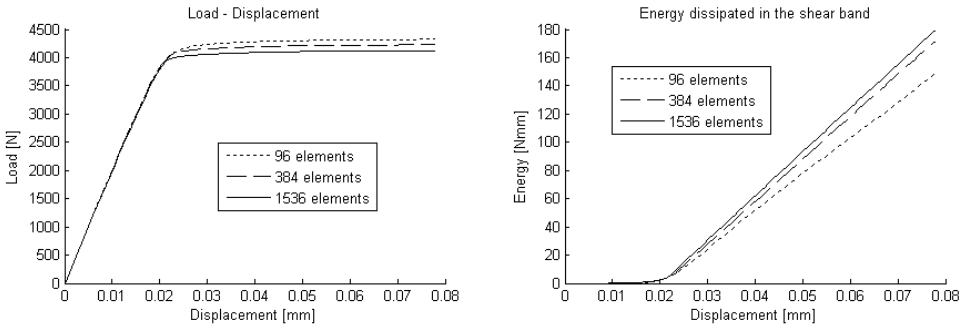

Figure 22

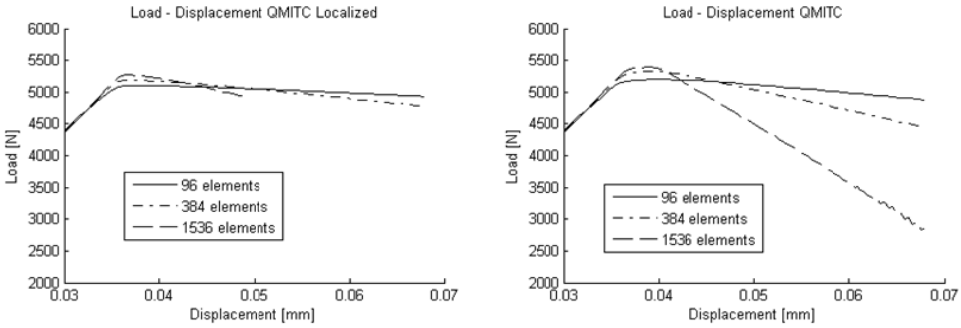
Load - Displacement QMITC Localized
Load [N]
Displacement [mm]
96 elements
384 elements
1536 elements
Load - Displacement QMITC
Load [N]
Displacement [mm]
96 elements
384 elements
1536 elements

Figure 23